



Eidgenössische Technische Hochschule Zürich
Swiss Federal Institute of Technology Zurich

Exploring Multi-bit Spike Trains in Neuromorphic Computing

Bachelor Thesis

Yi Zhu

Monday 20th January, 2025

Advisors: Dr. G. Kwasniewski, P. Okanovic, Prof. Dr. T. Hoefler
Department of Computer Science, ETH Zürich

Abstract

Spiking Neural Networks (SNNs) represent an emerging paradigm in machine learning, inspired by biological neurons, with potential for greater energy efficiency compared to traditional Artificial Neural Networks (ANNs). Unlike ANNs, which use continuous floating-point outputs, SNNs produce discrete (binary) spikes when a neuron's membrane voltage exceeds a threshold.

In this thesis we propose a novel firing model where neurons fire at multiple spiking levels (multi-bit spike trains) when their membrane potentials reach corresponding thresholds. We show that this model enables faster convergence and better performance on various tasks compared to the traditional 1-bit spike train model, while maintaining the energy efficiency of SNNs. We also present an energy consumption model in a real-world workflow and show how the multi-bit spike train model can be beneficial in terms of energy efficiency.

Contents

Contents	iii
1 Introduction	1
2 Background	3
2.1 Leaky Integrate-and-Fire Neuron Model	3
2.1.1 Dynamics of the Membrane Potential	3
2.1.2 Spiking Mechanism	4
2.2 Training of Spiking Neural Networks	4
2.2.1 Constructing Spiking Neural Networks	4
2.2.2 Backpropagation through Time	5
2.2.3 Surrogate Gradient	5
3 Multi-bit Spike Train Model	7
3.1 Graded Spikes	7
3.2 Shifted Surrogate Function	8
3.3 Implementation	8
4 Experiments	11
4.1 Convergence & Accuracy	11
4.2 Firing Rate	15
4.3 Quantizability	17
5 Evaluation	19
5.1 Energy Consumption	19
5.1.1 Training Energy Consumption on GPUs	19
5.1.2 Inference Energy Consumption on Neuromorphic Chips	20
5.1.3 Tradeoffs	21
5.2 Performance	23
6 Related Work	25

7 Concluding Remarks	27
7.1 Conclusion	27
7.2 Future Work	27
A Accuracy of the Multi-Bit Spike Train Model	29
A.1 Accuracy Curves	29
A.1.1 Fashion MNIST	29
A.1.2 MNIST	31
A.1.3 NMNIST	33
A.1.4 DVS Gesture	35
A.1.5 CIFAR-10	37
A.2 Iterations to Reach the Target Accuracy of 80%	39
A.2.1 Fashion MNIST	39
A.2.2 MNIST	39
A.2.3 NMNIST	40
A.2.4 DVS Gesture	40
A.2.5 CIFAR-10	41
B Firing Rate in Different Positions of the Multi-Bit Spike Train Model	43
B.1 Fashion MNIST	43
B.2 MNIST	44
B.3 NMNIST	46
B.4 DVS Gesture	48
B.5 CIFAR-10	50
C Energy Consumption Estimation	53
C.1 Training Energy Consumption Estimation on GPUs	53
C.1.1 Fashion MNIST	53
C.1.2 MNIST	53
C.1.3 NMNIST	54
C.1.4 DVS Gesture	55
C.1.5 CIFAR-10	55
C.2 Inference Energy Consumption Estimation on Neuromorphic Hardware	55
C.2.1 Fashion MNIST	56
C.2.2 MNIST	56
C.2.3 NMNIST	56
C.2.4 DVS Gesture	57
C.2.5 CIFAR-10	57
C.3 Trading Accuracy for Energy Consumption	58
C.3.1 Fashion MNIST	58
C.3.2 CIFAR-10	60

Contents

Bibliography	63
---------------------	-----------

Chapter 1

Introduction

Artificial neural networks (ANNs) [17] have been widely used in machine learning and artificial intelligence. The computational principle behind ANNs is mostly matrix multiplications which can be efficiently implemented on modern hardware like GPUs [19]. Although such operations can be excellently parallelized and accelerated, the energy consumption of ANNs is still high.

On the other hand, human brains are much more energy-efficient than ANNs. The energy consumption of the human brain is estimated to be around 20 watts [3], while the energy consumption of a large ANN model like ChatGPT is estimated to be around 23.5 megawatts [7]. The human brain is estimated to be over one million times more energy-efficient than ChatGPT. One of the reasons for this energy efficiency is the difference between the neuron models used in ANNs and the biological neurons in the human brain. Unlike ANNs, which use floating-point numbers for numerical computation, biological neurons communicate with each other using spike trains and rely on temporal information [11].

To model such biological neurons and deploy them in artificial neural networks, spiking neural networks (SNNs) have been proposed. The most commonly used neuron model in SNNs is the leaky integrate-and-fire (LIF) [14]. In this model, a neuron's membrane potential is increased by incoming spikes and decreased by a leak term. When the membrane potential reaches a threshold, the neuron fires a spike and resets its membrane potential. The communication between neurons in SNNs is done by sending spikes, which are binary events.

In this thesis, we propose a novel neuron model where neurons can fire at multiple spiking levels. Instead of firing a single spike when the membrane potential reaches a threshold, neurons can fire multiple spikes at different levels. We call this model the multi-bit spike train model. The motivation

1. INTRODUCTION

behind this model is to increase the communication bandwidth between neurons and enable more efficient training or inference in SNNs. We explore the properties of this model and compare it with the traditional LIF neuron model.

We experiment on various datasets and tasks with the multi-bit spike train model and show that it can achieve better performance than the classic 1-bit spike train model in the most cases. Finally, we also present a energy consumption model of the multi-bit spike train model and show that it can be more energy-efficient than the LIF neuron model assuming certain hardware implementations.

Chapter 2

Background

2.1 Leaky Integrate-and-Fire Neuron Model

2.1.1 Dynamics of the Membrane Potential

A leaky integrate-and-fire (LIF) neuron is a simple model of a neuron that captures the essential dynamics of a neuron. The LIF model is described by the differential equation:

$$\tau \frac{dU(t)}{dt} = -U(t) + I_{\text{in}}(t) \quad (2.1)$$

where $U(t)$ is the membrane potential of the neuron, τ is the time constant of the neuron, and $I_{\text{in}}(t)$ is the input current to the neuron. The neuron fires a spike when the membrane potential reaches a threshold U_{th} . The membrane potential is then reset to a reset potential U_{reset} .

The equation above has an approximate solution given by:

$$U[t] = \beta U[t - 1] + (1 - \beta) I_{\text{in}}[t] \quad (2.2)$$

where $\beta = e^{-\Delta t/\tau}$, Δt is the time step, and $I_{\text{in}}[t]$ is the input current at time t , defined by the following equation:

$$I_{\text{in}}[t] = W \cdot X[t] \quad (2.3)$$

where $X[t]$ is the input spike train at time t , and W is the weight matrix.

Since the weights W are learnable parameters, one often merges the weights with the coefficient $(1 - \beta)$. In the end, one obtains the following equation:

$$U[t] = \beta U[t - 1] + W \cdot X[t] - S_{\text{out}}[t] \cdot \theta \quad (2.4)$$

where $S_{\text{out}}[t]$ is the output spike train at time t , and θ is the threshold of the neuron. By subtracting $S_{\text{out}}[t] \cdot \theta$ from the equation, one resets the membrane potential (soft reset) when the neuron fires a spike.

2.1.2 Spiking Mechanism

The firing model, as defined by Lapicque in 1907, is modeled by the following equation:

$$S_{\text{out}}[t] = \begin{cases} 1 & \text{if } U[t] \geq \theta \\ 0 & \text{otherwise} \end{cases} \quad (2.5)$$

This is a heaviside step function, which is not differentiable.

For the simplicity of analysis, one often considers $x := U[t] - \theta$ and $y := S_{\text{out}}[t]$. At each time step, the membrane potential $U[t]$ is evaluated through

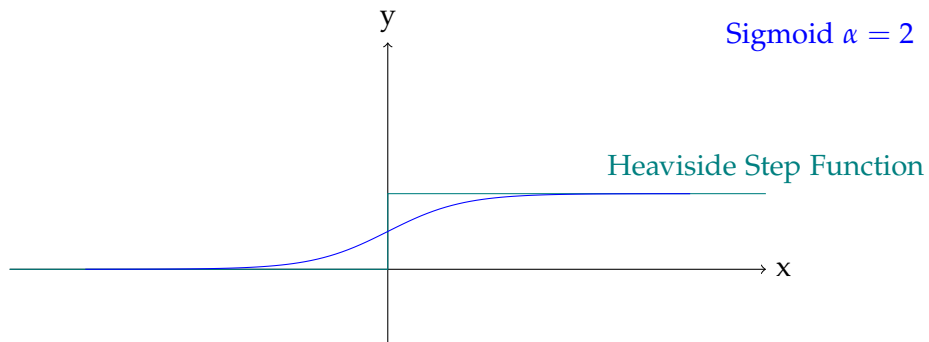


Figure 2.1: Comparison of the Heaviside Step Function and the Sigmoid Function

the Heaviside step function, and the output is a binary value of 0 or 1, illustrated in Figure 2.1. The array of these binary values in the time domain is called the spike train of the neuron.

After the neuron fires a spike, the membrane potential is reset to the resting potential. There are two ways to reset the membrane potential: hard reset and soft reset. In the hard reset, the membrane potential is immediately set to the resting potential. In the soft reset, the membrane potential is subtracted by the threshold when the neuron fires a spike. Although the hard reset is more biologically plausible and more efficient in terms of computation, the soft reset is more popular in practice because it often delivers better performance in training [9]. Here we focus on the soft reset.

2.2 Training of Spiking Neural Networks

2.2.1 Constructing Spiking Neural Networks

The construction of spiking neural networks is similar with the construction of traditional artificial neural networks. One of the most popular methods to construct a spiking neural network is to use the leaky integrate-and-fire (LIF) neuron node to replace the ReLU activation function in the ANNs.

There are also other techniques to replace some components of the ANNs with certain tweaks for the SNNs, e.g. variants of batch normalization (such as Spike-Norm [23]) and attention mechanisms (such as Spiking RWKV [27]), but they are outside of the scope of the thesis.

2.2.2 Backpropagation through Time

Although our brains are likely not trained by backpropagation, the gradient-based optimization is still the most popular and reliable method to train the neural networks.

Backpropagation through time (BPTT) is a method used to train recurrent neural networks (RNNs) by unfolding the network in time and applying backpropagation. The same method can be applied to train SNNs, as they are very similar to RNNs.

There are also other methods to train SNNs, like SLAYER [24] and EXODUS [4] which utilize the vectorized model of the SNNs. However, we will focus on the temporal model of the SNNs in this thesis.

2.2.3 Surrogate Gradient

Gradient-based optimization requires the activation function to be differentiable. However, the heaviside step function is not. Therefore, one often uses another differentiable function to approximate the Heaviside step function in the backpropagation algorithm [18], e.g. the sigmoid function (see Figure 2.1):

$$S'_{\text{out}}[t] = \frac{1}{1 + e^{-\alpha \cdot x}} \quad (2.6)$$

It turns out that SNNs can tolerate such approximations, and it has become the state-of-the-art method to train high-performant SNNs.

Chapter 3

Multi-bit Spike Train Model

3.1 Graded Spikes

Now we consider the firing model with graded spikes, namely our multi-bit spike train model. We divide the range of $[0, \theta]$ into $2^n - 1$ intervals where n is the number of bits used to encode one single spike. Then once the membrane potential reaches the threshold for a certain interval, the neuron fires a spike with the corresponding intensity described as follows:

$$S_{\text{out}}[t] = \begin{cases} 0 & \text{if } U[t] < \frac{1}{2^n-1} \cdot \theta \\ \frac{i}{2^n-1} & \text{if } \frac{i}{2^n-1} \cdot \theta \leq U[t] < \frac{i+1}{2^n-1} \cdot \theta, i \in [1, 2^n - 2] \\ 1 & \text{if } U[t] \geq \theta \end{cases} \quad (3.1)$$

When $n = 1$, the multi-bit spike train model becomes the binary spike train model.

Again we focus on the case $x := U[t] - \theta$ and $y := S_{\text{out}}[t]$, the spike function is now a step function with $2^n - 1$ steps, illustrated in Figure 3.1.

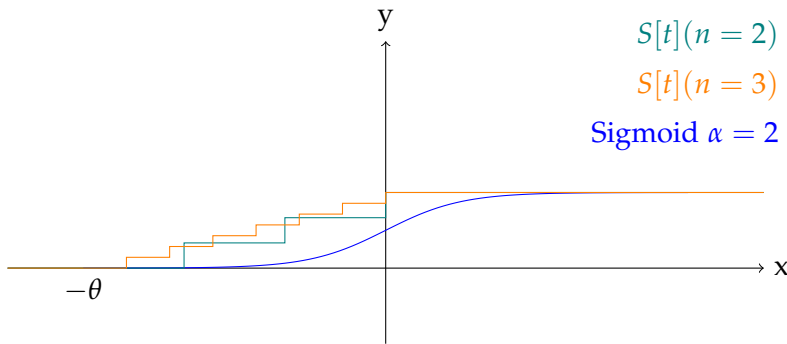


Figure 3.1: Comparison of the Multi-bit Spike Train Model and the Sigmoid Function

Intuitively this firing model enables higher information bandwidth between

3. MULTI-BIT SPIKE TRAIN MODEL

neurons. Although biologically, neurons can only fire binary encoded spikes, the spike trains can be rate encoding [12] or temporal encoding [5]. The rate encoding is based on the number of spikes in a certain time window, i.e. the neuron fires more spikes when the input is stronger. The temporal encoding is based on the timing of the spikes, i.e. the neuron fires earlier when the input is stronger.

The multi-bit spike train model is a generalization where the graded spikes can be interpreted as rate encoding and their temporal positions can be interpreted as temporal encoding.

3.2 Shifted Surrogate Function

The multi-bit spike train model leads to the problem that the surrogate function no longer approximates the spike function well. One can tell from gap between the multi-bit spike train model and the sigmoid function in Figure 3.1 that the gradients derived from the sigmoid function can no longer reflect the gradients of the multi-bit spike train model accurately. A simple solution is to shift the sigmoid function accordingly. The following equation describes the shifted sigmoid function:

$$S'_{\text{out}}[t] = \frac{1}{1 + \exp(-\alpha \cdot (x + \frac{2^{n-1}-1}{2^n-1} \cdot \theta))} \quad (3.2)$$

This technique centers the sigmoid function relatively to the multi-bit spike train model, illustrated in Figure 3.2. It improves the accuracy of the resulting networks.

3.3 Implementation

We use the SNN framework SpikingJelly which is based on PyTorch to implement the multi-bit spike train model. The firing mechanism is implemented as a forward path of the surrogate function in SpikingJelly. One just needs to override the Heaviside step function with the multi-bit spike train model. The core implementation is shown in Figure 3.3.

Noticing that the input x is already centered to zero by SpikingJelly, so we apply the shift directly to the sigmoid function.

3.3. Implementation

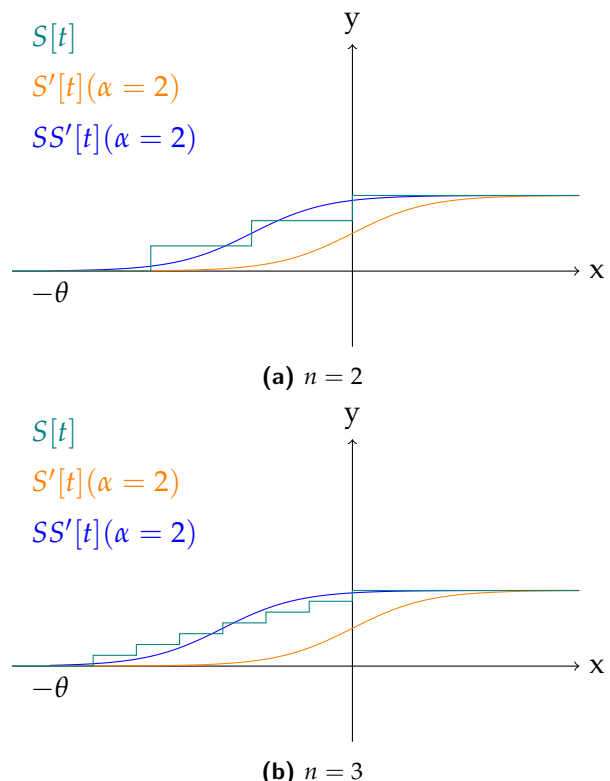


Figure 3.2: Comparison of Sigmoid Function, Shifted Sigmoid Function and Multi-bit Spike Train Model: $S[t]$ is the output spikes of the multi-bit spike train model, $S'[t]$ is the output spikes of the sigmoid function, $SS'[t]$ is the output spikes of the shifted sigmoid function

3. MULTI-BIT SPIKE TRAIN MODEL

```
@torch.jit.script
def multi_level(x: torch.Tensor, n: int, threshold: float):
    l = int(2**n)-1
    r = (x >= 0).float()
    for i in range(1, l):
        r += ((x >= -float(i)/l * threshold) ^ (x >= -float(i-1)/l * threshold)) * float(l-i)/l
    return r.to(x)

class sigmoid(torch.autograd.Function):
    @staticmethod
    def forward(ctx, x, alpha, n, threshold):
        shift = (2**n-1) / (2**n-1) * threshold
        if x.requires_grad:
            ctx.save_for_backward(x+shift)
            ctx.alpha = alpha
            ctx.n = n
            ctx.threshold = threshold
        return multi_level(x, n, threshold)

    @staticmethod
    def backward(ctx, grad_output):
        return sigmoid_backward(grad_output, ctx.
                               saved_tensors[0], ctx.alpha, ctx.n, ctx.threshold)

class Sigmoid(SurrogateFunctionBase):
    def __init__(self, alpha=4.0, spiking=True, n=1,
                 threshold=1.0):
        super().__init__(alpha, spiking, n, threshold)

    @staticmethod
    def spiking_function(x, alpha, n, threshold):
        return sigmoid.apply(x, alpha, n, threshold)

    @staticmethod
    def backward(grad_output, x, alpha, n, threshold):
        shift = (2**n-1) / (2**n-1) * threshold
        return sigmoid_backward(grad_output, x+shift, alpha,
                               n, threshold)[0]
```

Figure 3.3: Implementation of the Multi-bit Spike Train Model in SpikingJelly

Chapter 4

Experiments

We implement the multi-bit spike train model with SpikingJelly [10] (version 0.0.0.0.15) using its PyTorch [21] (version 2.5.0) backend. All experiments are conducted in the NVIDIA PyTorch container (nvcr.io/nvidia/pytorch:24.08-py3) on an NVIDIA GH200 super chip.

We compare the multi-bit spike train model with the traditional 1-bit spike train model on various tasks and datasets. The regular static datasets are imported from Torchvision [16] while the neuromorphic datasets are imported from Tonic [15].

We measure the training accuracy (per batch), test accuracy (per epoch) and firing rate at certain points in the networks of the 1-bit to 8-bit spike train models. We then investigate the convergence, accuracy, firing rate, and quantizability of the multi-bit spike train model.

We mainly use the Fashion MNIST dataset [26] and a convolutional neural network (CNN) to set up the experiments of an image classification task. We will also show the results also hold on more complex datasets like CIFAR-10 [13].

In the following sections, the input images from Fashion MNIST are first converted to spike trains using the Poisson encoding method. The CNN has a structure of $28 \times 28 - 8c5 - 2a - 16c5 - 2a - 10o$, visually illustrated in Figure 4.1.

4.1 Convergence & Accuracy

The first noticeable difference between the multi-bit spike train model and the 1-bit spike train model is the convergence speed (see Figure 4.2). Even just by increasing the bit width of the spike train from 1 to 2, the convergence speed of the network is significantly improved.

4. EXPERIMENTS

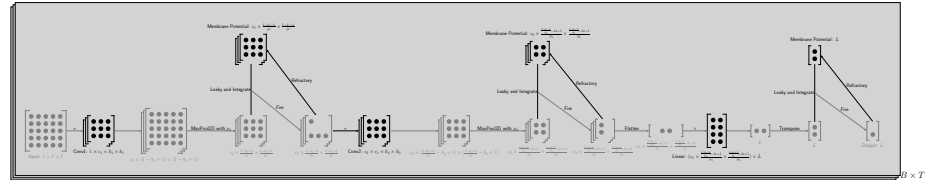
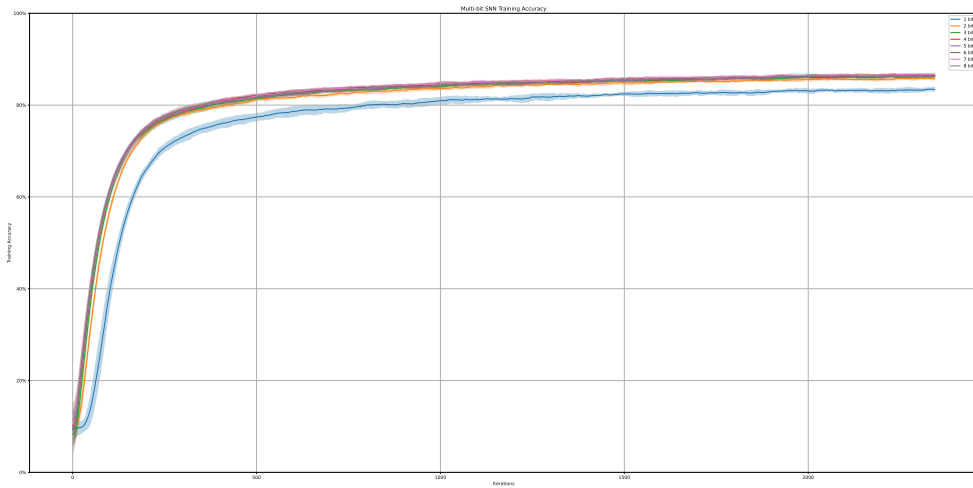
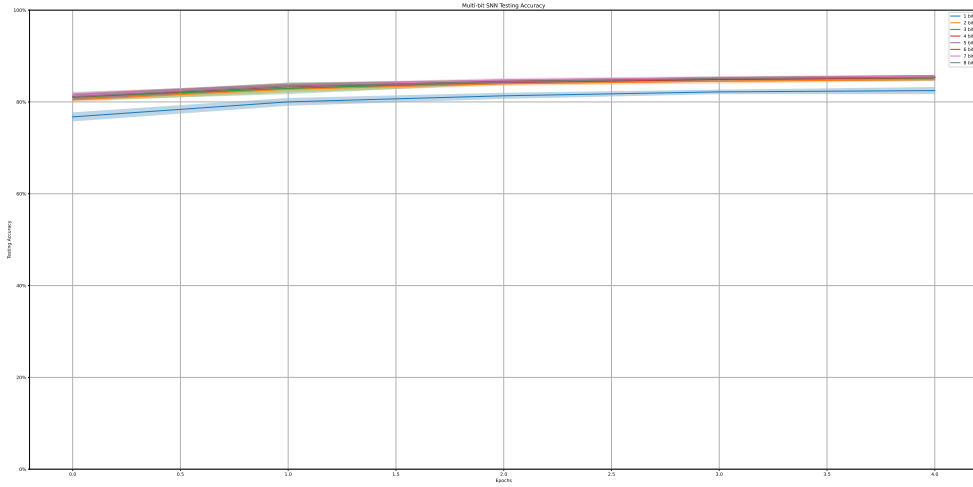


Figure 4.1: The CNN structure used in the experiments with Fashion MNIST dataset



(a) Training Accuracy (smoothed with a window size of 100)



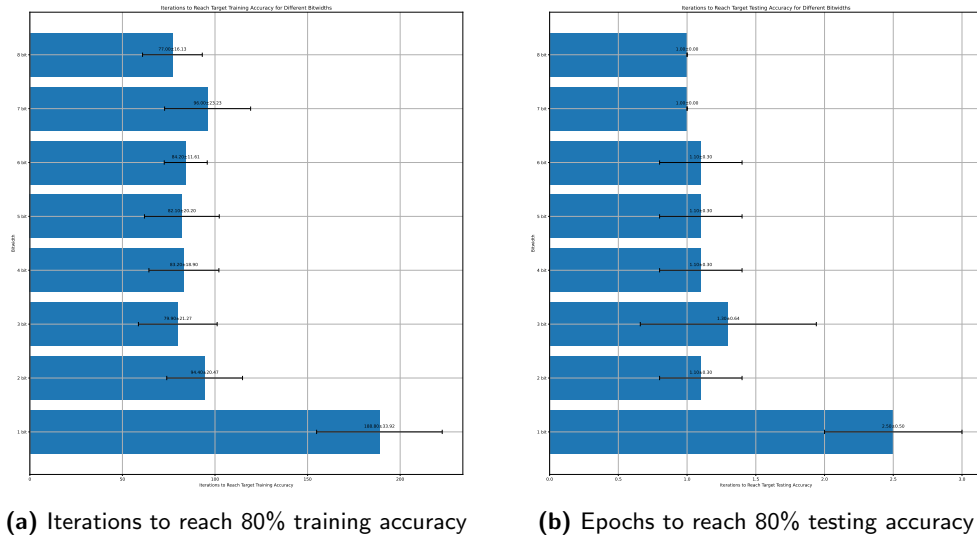
(b) Test Accuracy

Figure 4.2: Comparison of the Convergence Speed of 1-bit to 8-bit Spike Train Model, repetition of the experiment 10 times

4.1. Convergence & Accuracy

The improvement in convergence speed can lead to significant reduction in the training time if considering a fixed target accuracy, especially considering the diminishing return of the training time with respect to the target accuracy.

Here we set the target accuracy to be 80%. The training time of the multi-bit spike train model is reduced by around 50%, shown in Figure 4.3.



(a) Iterations to reach 80% training accuracy

(b) Epochs to reach 80% testing accuracy

Figure 4.3: Comparison of the Training Time of 1-bit to 8-bit Spike Train Model, repetition of the experiment 10 times

Such improvement however also comes at certain cost:

- The improvement in convergence speed diminishes as the bit width of the spike train increases. The improvement from 2-bit to 3-bit ($\sim 15.4\%$) or even higher bit width (at most $\sim 59.2\%$ reduction in iterations compared to the 1-bit baseline) is not as significant as the improvement from 1-bit to 2-bit ($\sim 50\%$ reduction in iterations).
- The more complicated the model is, the harder is it to train the multi-bit spike train model. One can easily run into the problem of overfitting, for example in the case of DVS gesture recognition task A.1.4.

Due to the faster convergence speed, the multi-bit spike train model can achieve better accuracy than the 1-bit spike train model given a fixed number of iterations or epochs for the most cases (see Figure 4.4).

In general, such behaviors can be shown on MNIST [8], NMNIST [20], Fashion MNIST, DVS gesture recognition [2], and CIFAR-10 datasets (see Appendix A).

4. EXPERIMENTS

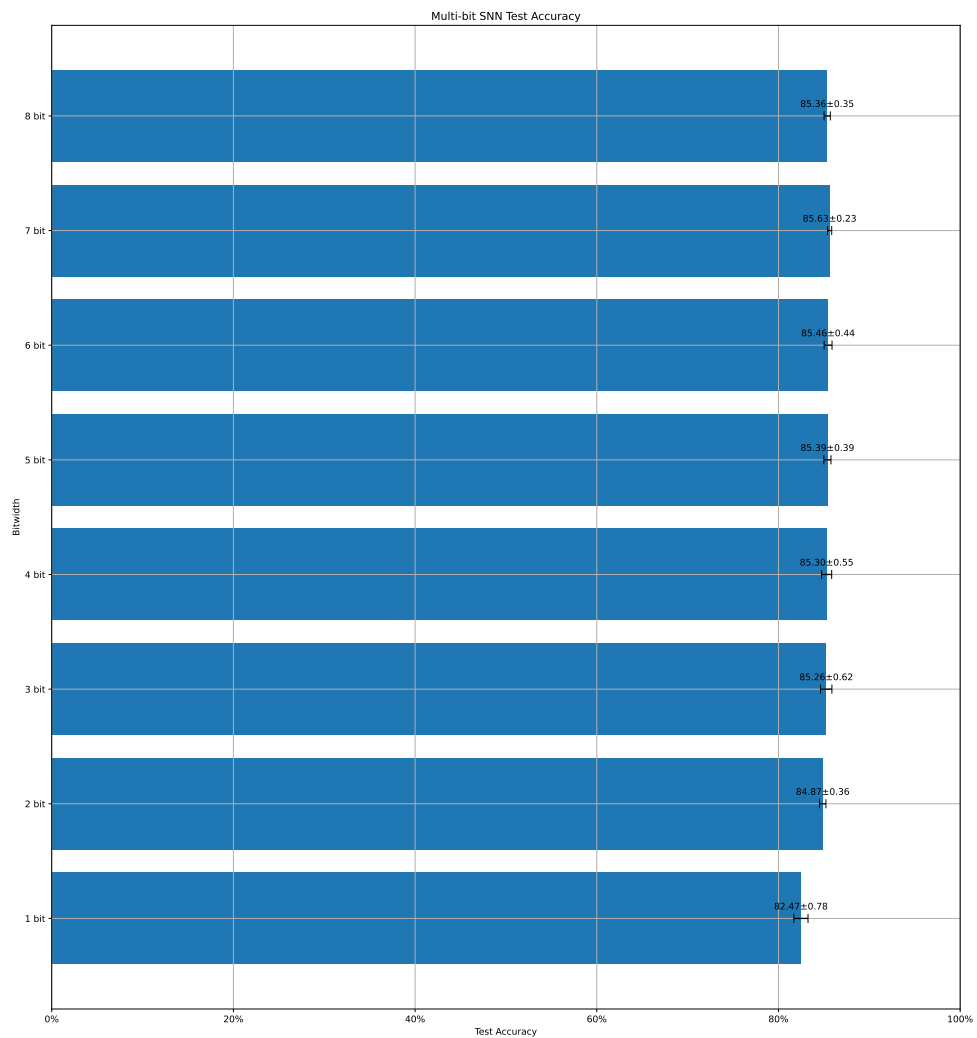


Figure 4.4: Comparison of the Final Accuracy of 1-bit to 8-bit Spike Train Model after 5 epochs, repetition of the experiment 10 times

4.2 Firing Rate

SNNs are known for their sparsity in the firing rate of the neurons. Here we notice that the multi-bit spike train model has a higher firing rate than the 1-bit spike train model (see Figure 4.5), as tradeoff for the improvement in convergence speed.

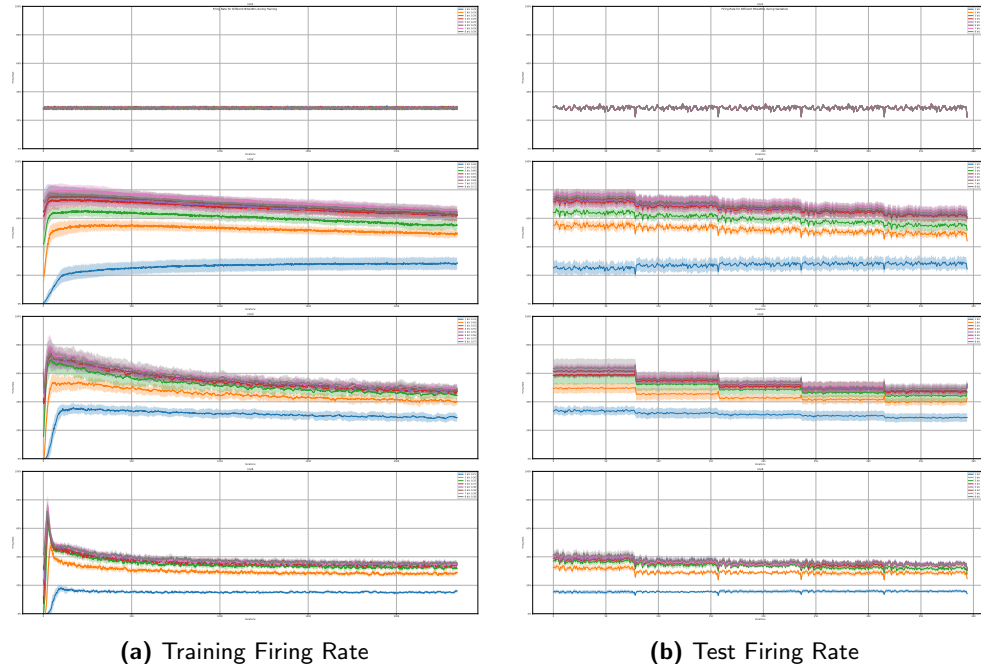


Figure 4.5: Comparison of the Firing Rate of 1-bit to 8-bit Spike Train Model: repetition of the experiment 10 times, "nnz[i]" means the number of non-zero elements in the i -th measuring point, corresponding to the position from the inputs to the output layer, "nnz1" is the input data

One can notice that the firing rate of the multi-bit spike train model peaks at the very beginning of the training session, when the model converges rapidly. The firing rate then decreases as the training progresses. If we extend the training session, the firing rate of the multi-bit spike train model tends to converge to the firing rate of the 1-bit spike train model. Such process takes however a long time (see Figure 4.6).

In the end, the firing rate of the multi-bit spike train model is comparable to the 1-bit spike train model (see Figure 4.7).

Such behavior is more visible on simpler datasets like MNIST. For now, we do not have any explanation for this phenomenon (see Appendix B).

4. EXPERIMENTS

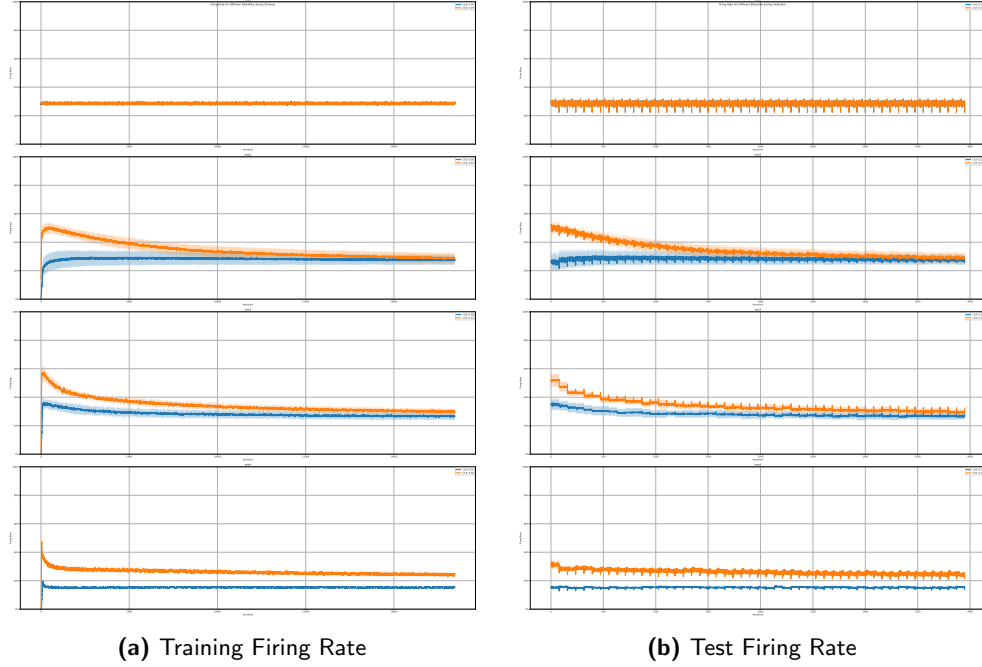


Figure 4.6: Analog to figure 4.5, but with a training session of 50 epochs instead of 5 epochs, only the 1-bit and 2-bit spike train models

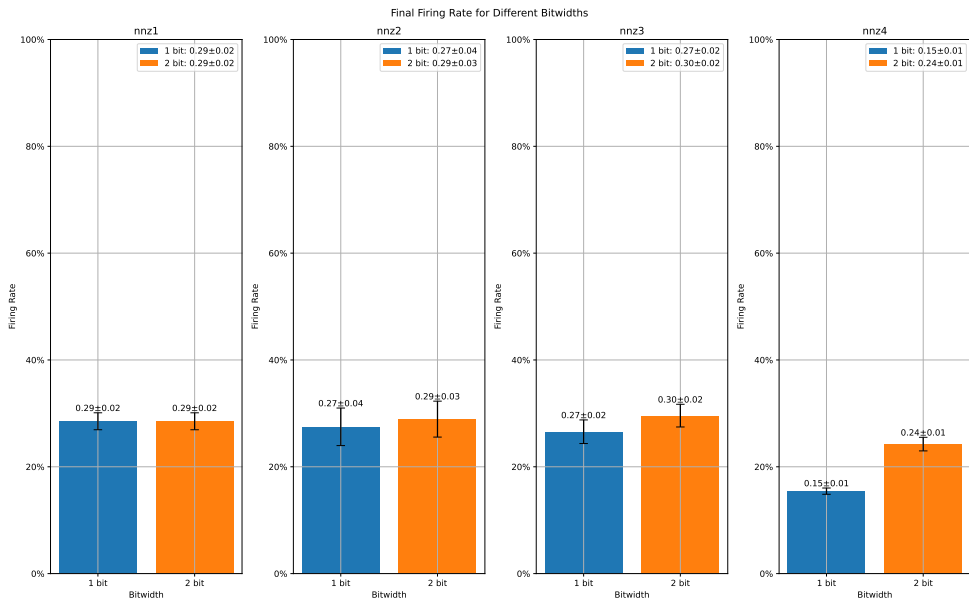


Figure 4.7: Comparison of the Final Firing Rate of 1-bit to 8-bit Spike Train Model after 50 epochs, only the 1-bit and 2-bit spike train models

4.3 Quantizability

A common technique to reduce the memory footprint of SNNs without having significant impact on accuracy is quantization [22]. There are studies showing that the weights and activations of SNNs can be quantized to 1-bit or 2-bit without significant loss in accuracy [25]. Here we show that both the multi-bit spike train model and the 1-bit spike train model can be trained with `bf16` and quantized to `int8` without significant loss in accuracy.

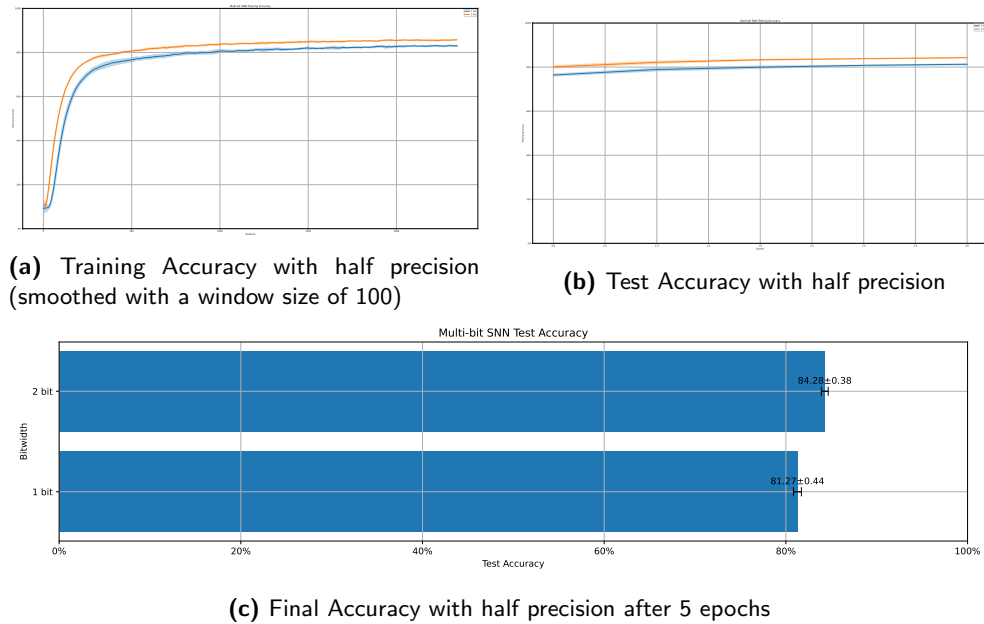


Figure 4.8: Comparison of the Convergence Speed of 1-bit to 8-bit Spike Train Model with half precision, repetition of the experiment 10 times

As shown in Figure 4.8, both SNN models converge well as if they were trained with `float32`. Meanwhile the multi-bit spike train model has its advantage in the convergence speed and accuracy preserved.

Before quantizing the models to `int8`, we first apply quantization-aware training to both SNN models. While regular ANNs may encounter various problems, both SNN models here converge well. We also see that the multi-bit spike train model has a faster convergence speed and better accuracy than the 1-bit spike train model (Figure 4.9).

We then quantize the weights and biases to `int8` using the PyTorch quantization API. The quantization of the LIF layer is not supported at the moment. We evaluate the quantized models on the test set. The final accuracy is barely affected by the quantization (see Figure 4.9c).

4. EXPERIMENTS

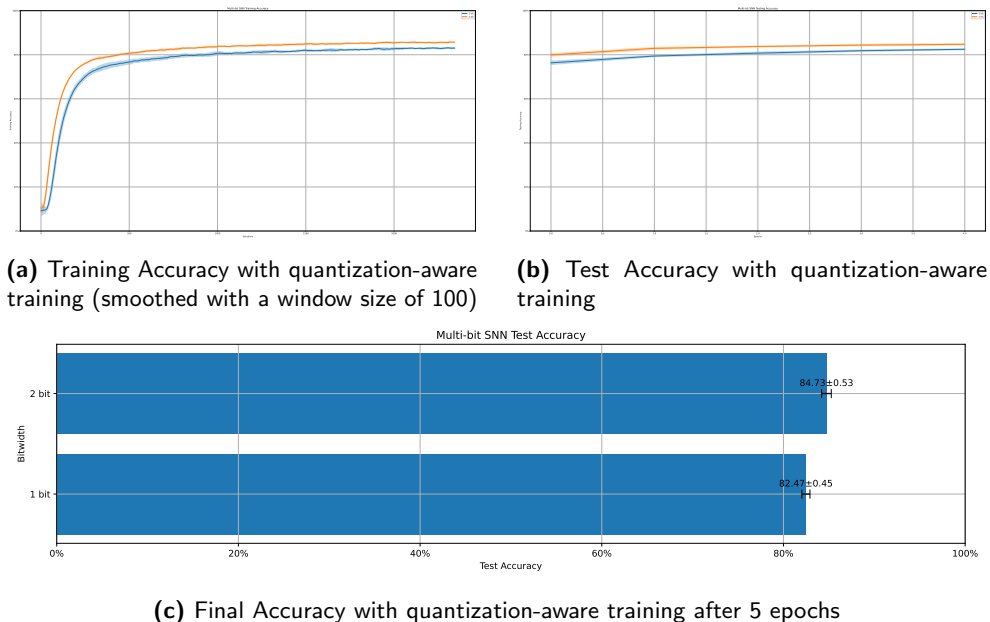


Figure 4.9: Comparison of the Convergence Speed of 1-bit to 8-bit Spike Train Model with quantization-aware training, repetition of the experiment 10 times

Chapter 5

Evaluation

5.1 Energy Consumption

One of the main motivations for SNNs is their energy efficiency compared to ANNs on specialized hardware. Products like Loihi from Intel [6] and TrueNorth from IBM [1] have proved the potential of SNNs by utilizing the asynchronous communication via spikes. In the real-world scenario, one often uses accelerators like GPUs to train SNNs and deploy them on specialized hardware to achieve fast training and energy efficient inference.

Here we present an energy consumption model for the multi-bit spike train model and compare it with the 1-bit spike train model. We consider the unique properties of various hardware implementations and give the energy consumption of the multi-bit spike train model relative to the 1-bit spike train model.

5.1.1 Training Energy Consumption on GPUs

On GPUs, low precision spikes are generally not very meaningful, as the hardware is not designed for such level mixed precision operations. Often the spikes are represented as 32-bit floating point numbers, which can be computed with the weights with the same precision. And the popular SNN frameworks like snnTorch and SpikingJelly do not utilize the sparsity of the spike trains. So here, the firing rate and the bit width of the spike train do not affect the energy consumption of the training phase.

The only factors that matter are the number of iterations required to reach a certain accuracy and the number of time steps that the network is simulated, assuming fixed network topology and batch size.

This allows us to create a simple, yet effective energy consumption model for the training phase on the GPUs. Let T_i denote the number of time steps,

5. EVALUATION

S_i denote the number of iterations required to reach a certain accuracy, and $E_{\text{train}-i}$ denote the energy consumption. Then we have:

$$E_{\text{train}-i} = T_i \cdot S_i \cdot c \quad (5.1)$$

where as c is a constant factor that depends on the hardware and the software used, however remains the same across different bit widths of the spike train.

As noticed in Section 4.1, one requires fewer iterations to reach a certain accuracy with the multi-bit spike train model. Here we focus on the energy consumption of the 2-bit spike train model, as it does not increase the firing rate as much as the other higher bit width models while still providing a significant improvement in convergence speed and accuracy.

Based on the results in Section 4.3, we can estimate the energy consumption of the 2-bit spike train model relative to the 1-bit spike train model directly by comparing the number of iterations required to reach a certain accuracy which is around $50.00 \pm 10.84\%$ in this case (see Figure 5.1).

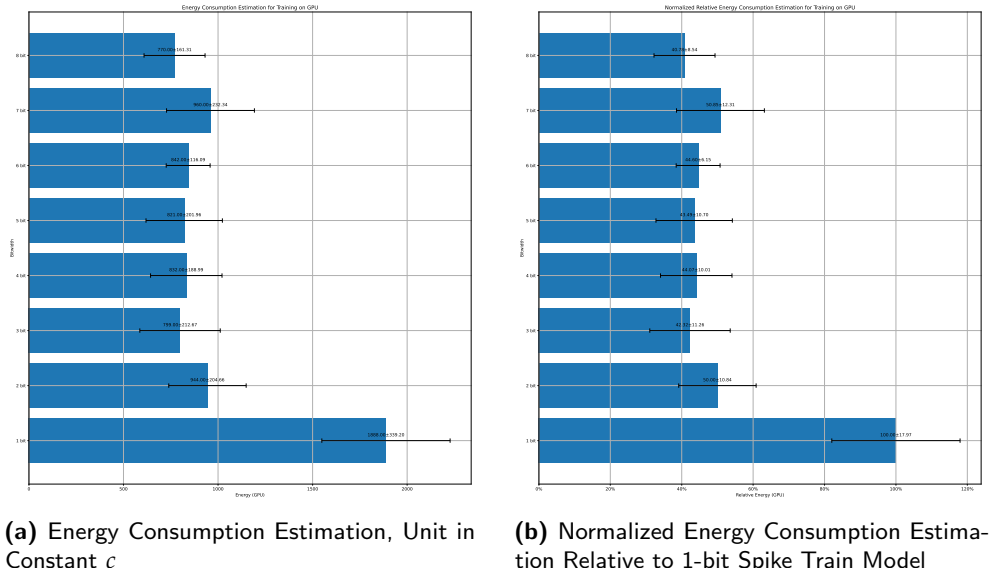


Figure 5.1: Training Energy Consumption Estimation on GPUs for Fashion MNIST Dataset

See more in Appendix C.1.

5.1.2 Inference Energy Consumption on Neuromorphic Chips

A widely adopted energy estimation model for neuromorphic chips is the following:

$$E_{\text{inference}} = F \cdot fr \cdot E_{\text{AC}} \cdot T \quad (5.2)$$

where F is the number of floating point operations required to simulate the network, fr is the firing rate of the neurons, E_{AC} is the energy consumption of accumulation, and T is the number of time steps.

It is however hard to evaluate the energy consumption of the multi-bit spike train model on neuromorphic chips like Loihi and TrueNorth, as they do not support multi-bit spikes natively. Although it may be possible to encode the multi-bit spikes into multiple spikes with different intensities, the energy consumption of such encoding is very expensive due to the high cost of the synchronization barrier between the time steps.

A viable option is to consider hardware like Intel Loihi 2 which supports graded spikes up to 32-bit precision. We consider the case of Intel Loihi 2 and make the following assumptions:

1. There is no difference in the energy consumption for the number of bits used to encode the spikes.
2. The energy consumption for a floating point operation is always E_{MAC} (Multiply-Accumulate).

Since the payload is not variable in this case, the energy consumption of the multi-bit spike train model is directly proportional to the firing rate given fixed maximum floating point operations and time steps. Analog as the equation 5.2, we have the following estimation for the i -bit spike train model:

$$E_{\text{inference}-i} = F \cdot fr_i \cdot E_{MAC} \cdot T_i \quad (5.3)$$

We can estimate the energy consumption of the 2-bit spike train model relative to the 1-bit spike train model by comparing the firing rate of the neurons. As expected, the energy consumption of the multi-bit spike train model is higher than the 1-bit spike train model, as the firing rate of the neurons is higher (see Figure 5.2).

See more in Appendix C.2.

5.1.3 Tradeoffs

One can tell that the energy consumption of the multi-bit spike train model has no direct advantage over the 1-bit spike train model on neuromorphic chips, as the firing rate of the multi-bit spike train model tends to be higher than the 1-bit spike train model. Moreover, one can also argue that the energy consumption from E_{MAC} is due to the graded spikes, which is not an issue with binary spikes.

We consider the energy consumption of the multi-bit spike train model in general as an opportunity to enable tradeoffs. If the inference is not the bottleneck of the application, then one can rely on the fast convergence speed

5. EVALUATION

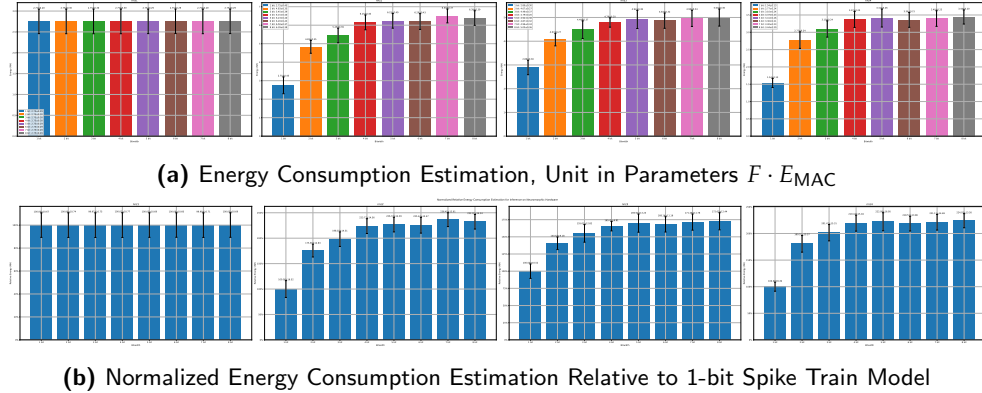


Figure 5.2: Inference Energy Consumption Estimation on Intel Loihi 2 for Fashion MNIST Dataset

of the multi-bit spike train model during training. If the inference is the bottleneck, then one can choose to train the multi-bit spike train model for longer time to achieve a firing rate that is comparable to the 1-bit spike train model (see Figure 5.3). Such tradeoffs are not possible with the 1-bit spike train model.

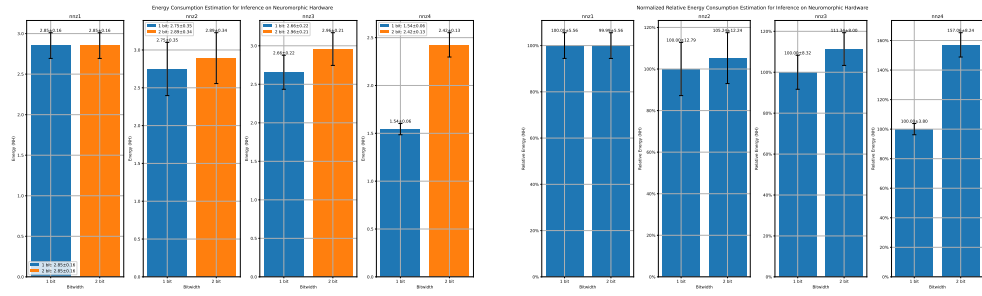


Figure 5.3: Inference Energy Consumption Estimation on Intel Loihi 2 for Fashion MNIST Dataset with 50 Training Epochs

And more interestingly, if one is satisfied with the accuracy of the 1-bit spike train model, then one can choose to train the multi-bit spike train model for fewer time steps. This can enable higher efficiency in both training and inference.

We take again the example of Fashion MNIST dataset, while $T = 10$ is a good choice for both the 1-bit and 2-bit spike train model, we can reduce the time steps to $T = 4$ for the 2-bit spike train model and still achieve a comparable accuracy (see 5.4).

5.2. Performance

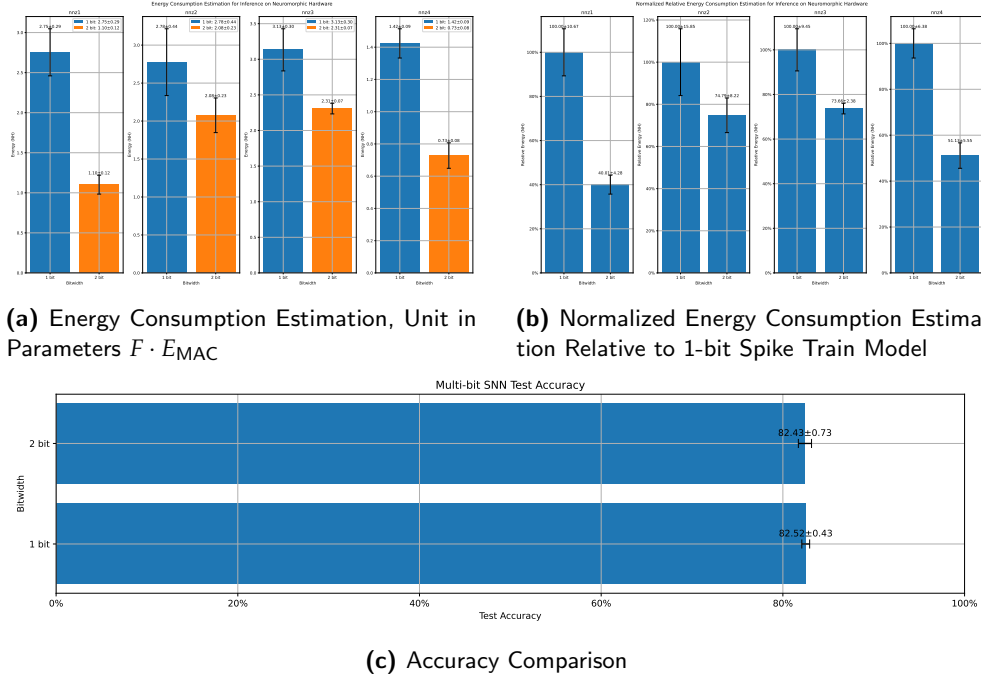


Figure 5.4: Inference Energy Consumption Estimation on Intel Loihi 2 and Test Accuracy for Fashion MNIST Dataset with 10 Time Steps for 1-bit Spike Train Model and 4 Time Steps for 2-bit Spike Train Model

See more in Appendix C.3.

This can lead to a significant reduction in the energy consumption. It may not be reflected as a direct advantage in the energy consumption model mentioned above 5.1.2, but in practice, it should bring significant benefits, as most of the neuromorphic chips are designed to utilize the asynchronous communication via spikes, so they do not have a central clock system to synchronize the time steps very efficiently, and the cost for the synchronization barrier is very high. As reference, the latency per tile hop on Intel Loihi is at most around 6.5 ns where as the latency for the synchronization barrier is from 113-465 ns.

5.2 Performance

In the section 5.1.1, we claim that the energy consumption on the GPUs are not affected by the firing rate and the bit width of the spike train in theory. However, in practice, with the increase of the bit width of the spike train, the training process slows down. This can be caused by the inefficient implementation of the multi-bit spike train model and the low level optimization on operations of sparse matrix multiplication.

5. EVALUATION

There is sufficient room for improvement, e.g. by utilizing the sparsity of the spike trains or completely switching to the vectorized model instead of the temporal model instead, which is shown to be more efficient with learning algorithms like SLAYER and EXODUS.

Chapter 6

Related Work

Chapter 7

Concluding Remarks

7.1 Conclusion

In this thesis we have developed a novel spike train model for spiking neural networks (SNNs) that uses multi-bit spikes to encode the information. We implement it using an SNN framework, SpikingJelly, based on PyTorch. And we have shown that the multi-bit spike train model can significantly improve the convergence speed and accuracy of the network compared to the traditional 1-bit spike train model while preserving other characteristics of the 1-bit spike train model such as high quantizability and low energy consumption. We consider the tradeoffs the multi-bit spike train model can bring in terms of energy consumption and performance important for maximizing the efficiency of SNNs on various hardware platforms.

7.2 Future Work

The multi-bit spike train model is a promising direction for the development of SNNs. However, there are still many open questions and challenges that need to be addressed in the future. Here we list some of the possible future work:

- **Optimization of the multi-bit spike train model:** The current implementation of the multi-bit spike train model is not optimized for performance. One can consider using just-in-time (JIT) compilation to improve the performance of the model.
- **Investigation of the overfitting problem:** The multi-bit spike train model is more complicated than the 1-bit spike train model, which can lead to overfitting. One can investigate the overfitting problem and propose solutions to mitigate it.

7. CONCLUDING REMARKS

- **Extension to other tasks and datasets:** The experiments in this thesis are mainly focused on image classification tasks. One can extend the multi-bit spike train model to other tasks and datasets to evaluate its performance.
- **Implementation on neuromorphic chips:** The multi-bit spike train model is designed to be hardware-friendly in theory. It would be more convincing if one can implement the model on neuromorphic chips like Intel Loihi 2 to evaluate its performance on specialized hardware.
- **Investigation of the energy consumption model:** The energy consumption model presented in this thesis is a simple estimation. One can investigate the energy consumption of the multi-bit spike train model more thoroughly and propose a more accurate model. Ideally, one can also measure the energy consumption of the multi-bit spike train model after implementing it on neuromorphic chips.

Appendix A

Accuracy of the Multi-Bit Spike Train Model

A.1 Accuracy Curves

A.1.1 Fashion MNIST

Launch command:

```
python -m test --N 8 --R 10 --T 10 --acc 0.80 --model
    FashionMNISTNet --data-path /scratch/zhiyi/codeSpace/data --
    dataset FashionMNIST --batch-size 128 --opt adam --lr 2e-3
    --lr-scheduler none --epochs 5 --lr-warmup-epochs 0 --
    output-dir /scratch/zhiyi/codeSpace/MultibitSpikes --mixup-
    alpha 0.0 --cutmix-alpha 0.0 --label-smoothing 0.0 --
    disable-amp
```

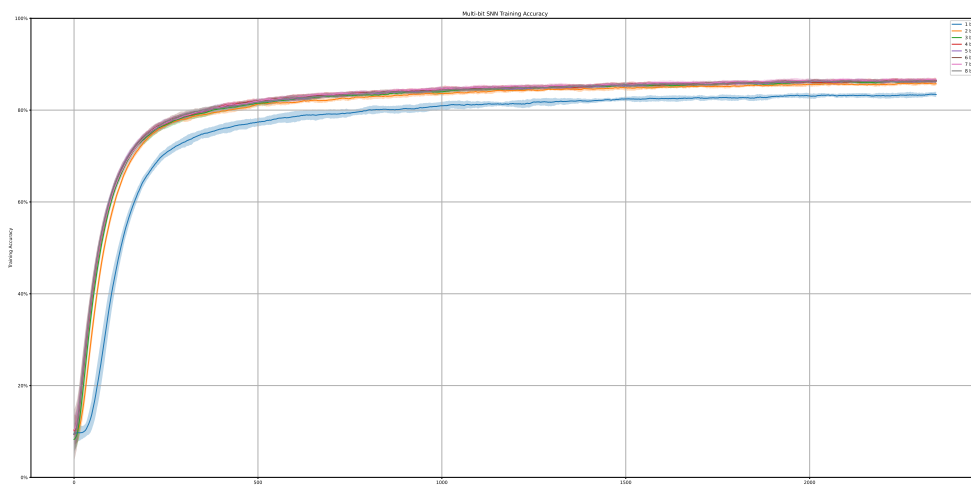


Figure A.1: Training Accuracy (smoothed with a window size of 100)

A. ACCURACY OF THE MULTI-BIT SPIKE TRAIN MODEL

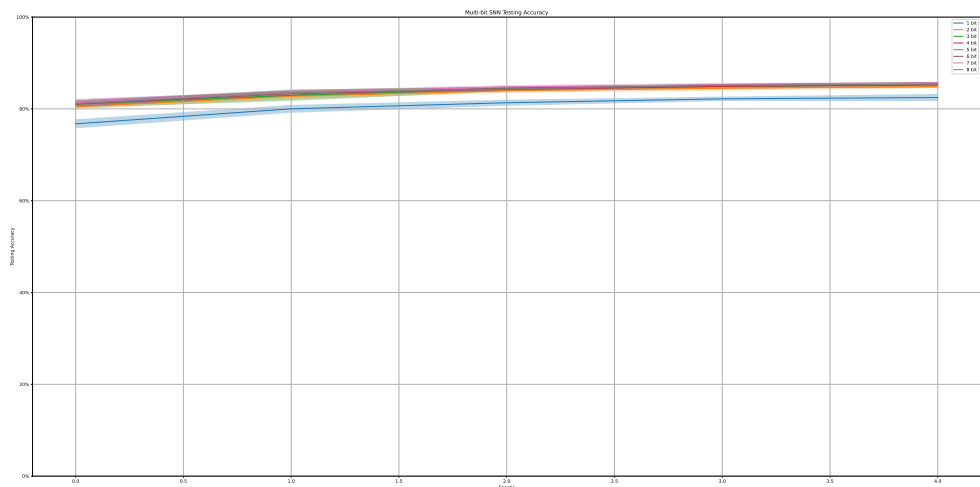


Figure A.2: Test Accuracy

A.1. Accuracy Curves

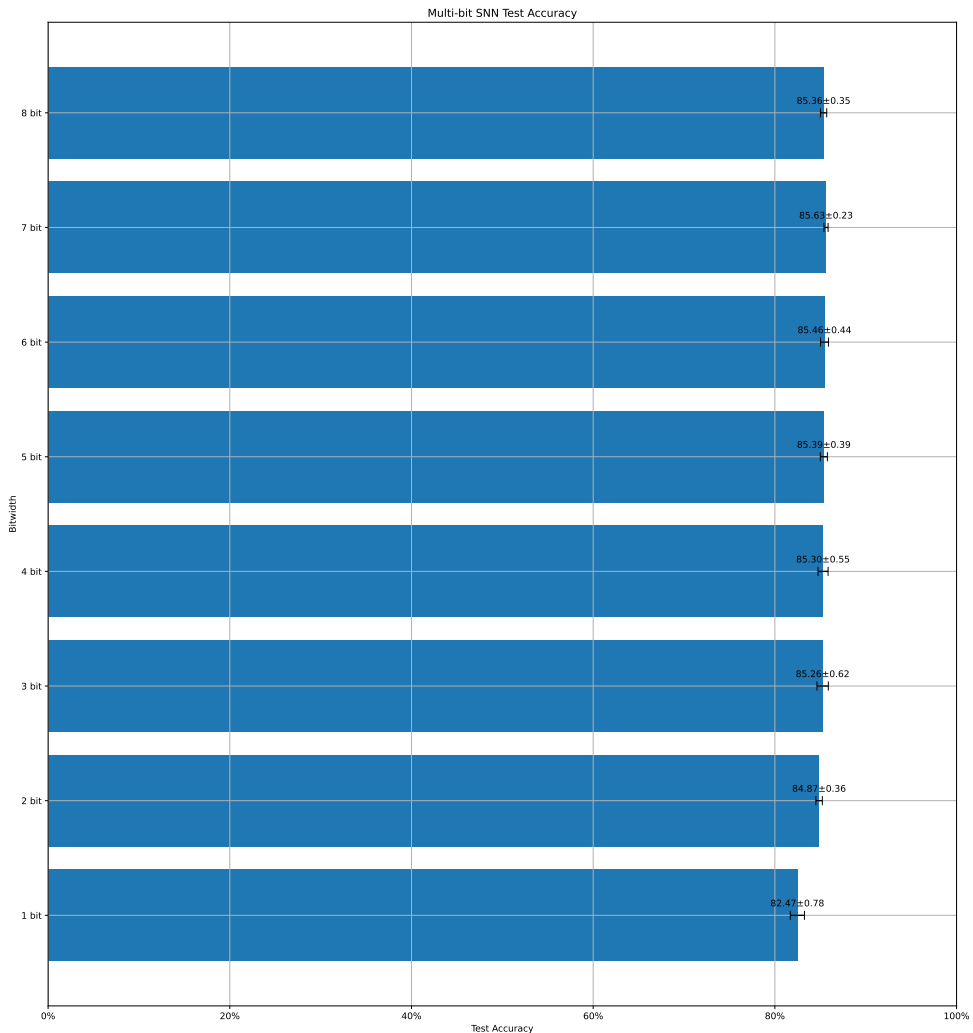


Figure A.3: Final Test Accuracy

A.1.2 MNIST

Launch command:

```
python -m test --N 8 --R 10 --T 10 --acc 0.80 --model  
    MNISTNet --data-path /scratch/zyi/codeSpace/data --dataset  
        MNIST --batch-size 128 --opt adam --lr 2e-3 --lr-  
        scheduler none --epochs 5 --lr-warmup-epochs 0 --output-  
        dir /scratch/zyi/codeSpace/MultibitSpikes --mixup-alpha  
        0.0 --cutmix-alpha 0.0 --label-smoothing 0.0 --disable-amp
```

A. ACCURACY OF THE MULTI-BIT SPIKE TRAIN MODEL

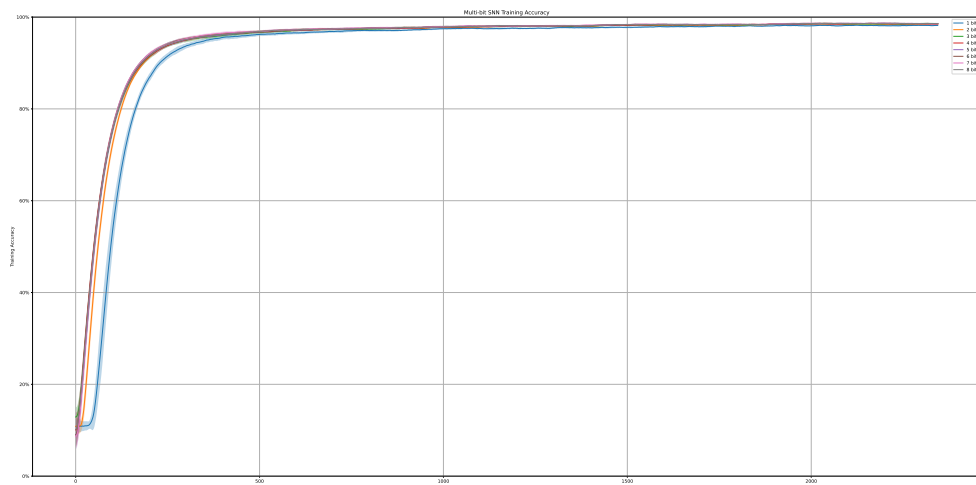


Figure A.4: Training Accuracy (smoothed with a window size of 100)

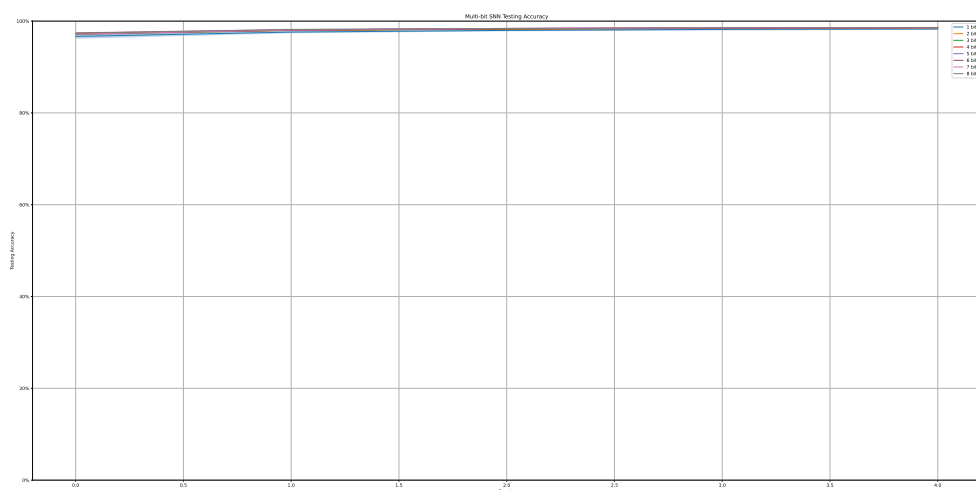


Figure A.5: Test Accuracy

A.1. Accuracy Curves

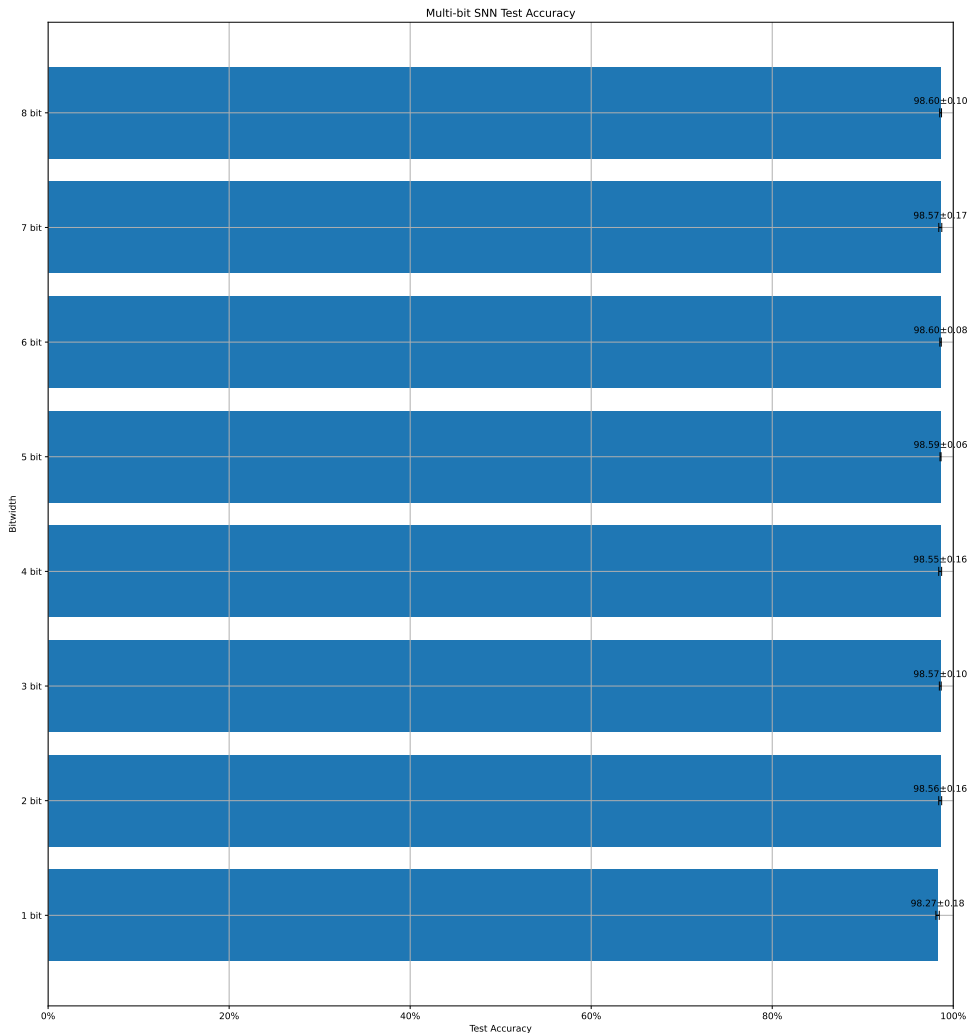


Figure A.6: Final Test Accuracy

A.1.3 NMNIST

Launch command:

```
python -m test --N 8 --R 10 --T 10 --acc 0.80 --model  
NMNISTNet --data-path /scratch/zyi/codeSpace/data --  
dataset NMNIST --batch-size 128 --opt adam --lr 2e-3 --lr-  
scheduler none --epochs 5 --lr-warmup-epochs 0 --output-  
dir /scratch/zyi/codeSpace/MultibitSpikes --mixup-alpha  
0.0 --cutmix-alpha 0.0 --label-smoothing 0.0 --disable-amp
```

A. ACCURACY OF THE MULTI-BIT SPIKE TRAIN MODEL

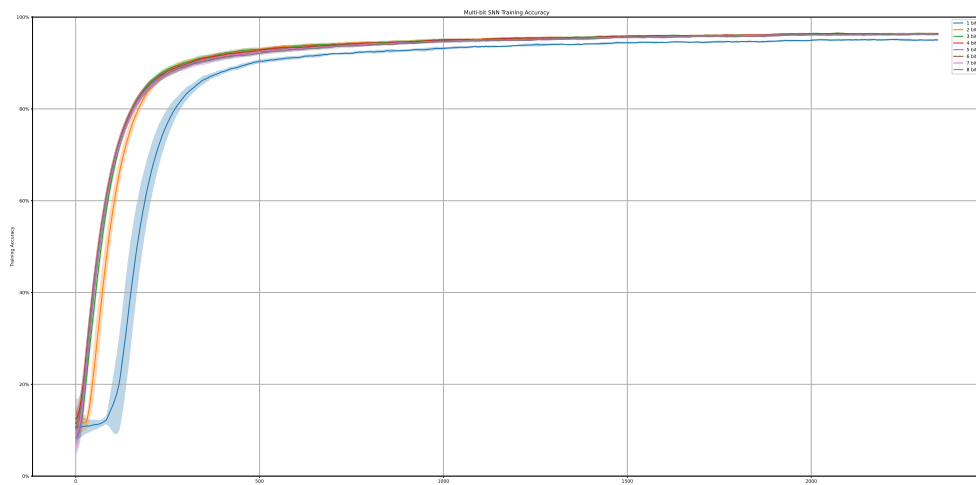


Figure A.7: Training Accuracy (smoothed with a window size of 100)

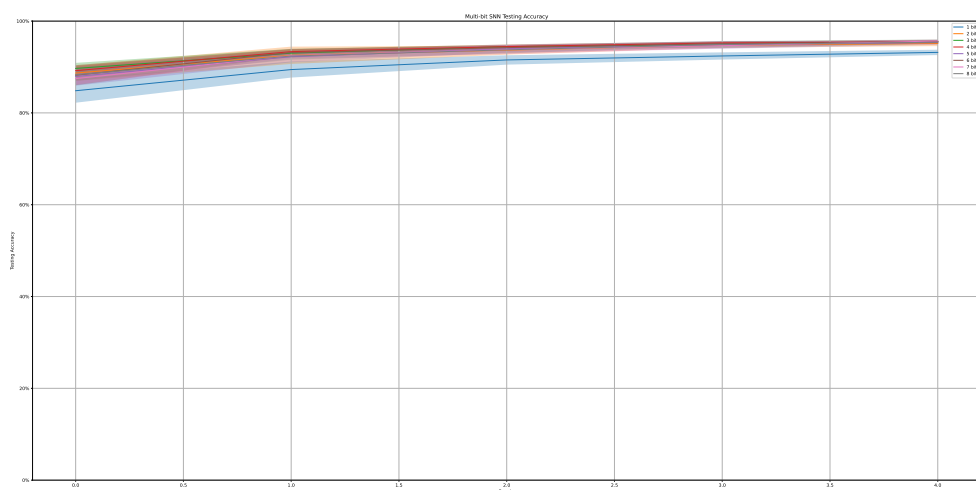


Figure A.8: Test Accuracy

A.1. Accuracy Curves

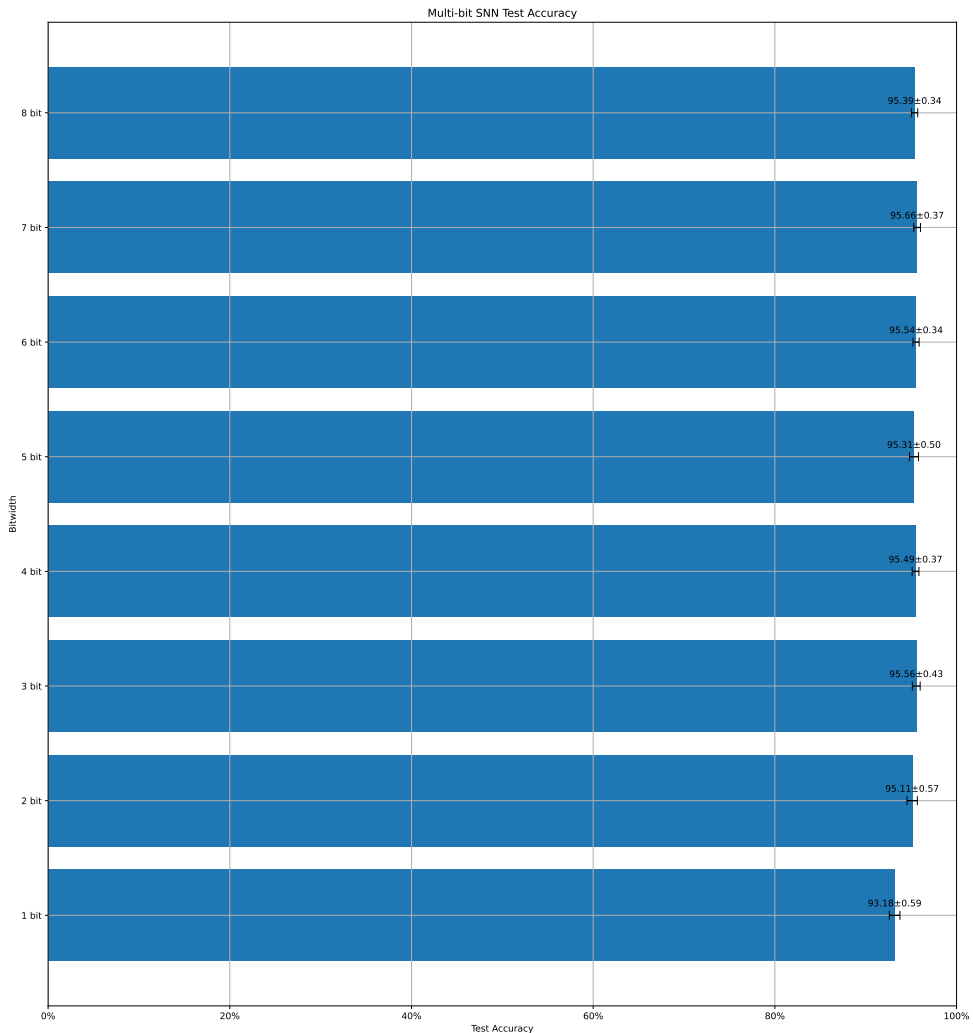


Figure A.9: Final Test Accuracy

A.1.4 DVS Gesture

Launch command:

```
python -m test --N 8 --R 10 --T 10 --acc 0.80 --model
    DVSGestureNet --data-path /scratch/zyi/codeSpace/data --
        dataset DVSGesture --batch-size 128 --opt adam --lr 1e-3
        --lr-scheduler cosa --epochs 20 --lr-warmup-epochs 0 --
        output-dir /scratch/zyi/codeSpace/MultibitSpikes
```

A. ACCURACY OF THE MULTI-BIT SPIKE TRAIN MODEL

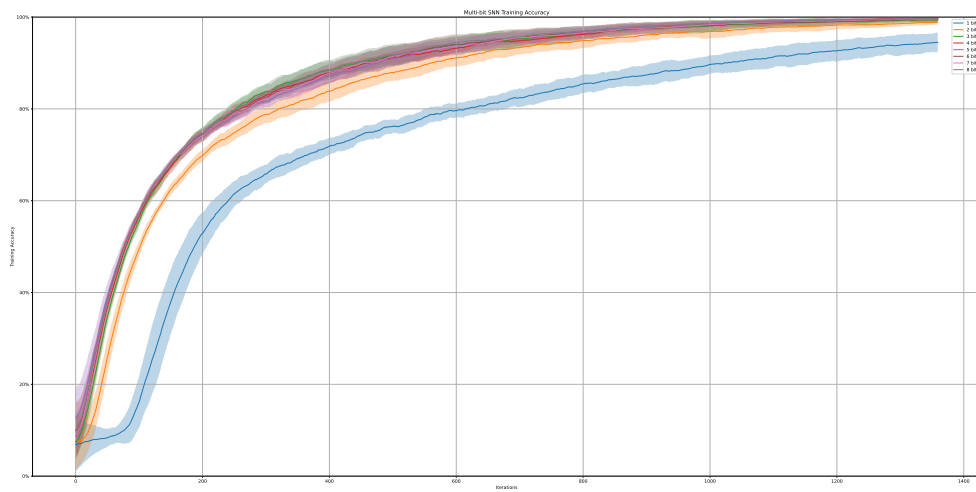


Figure A.10: Training Accuracy (smoothed with a window size of 100)

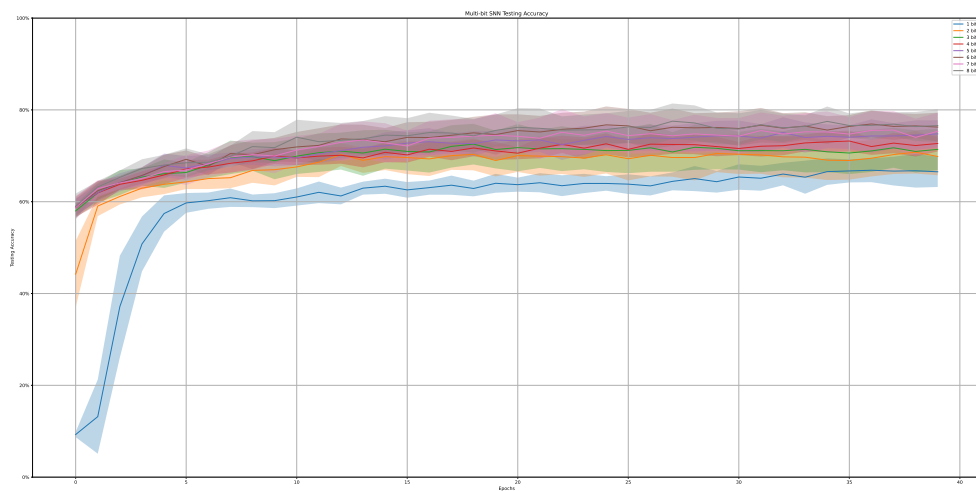


Figure A.11: Test Accuracy

A.1. Accuracy Curves

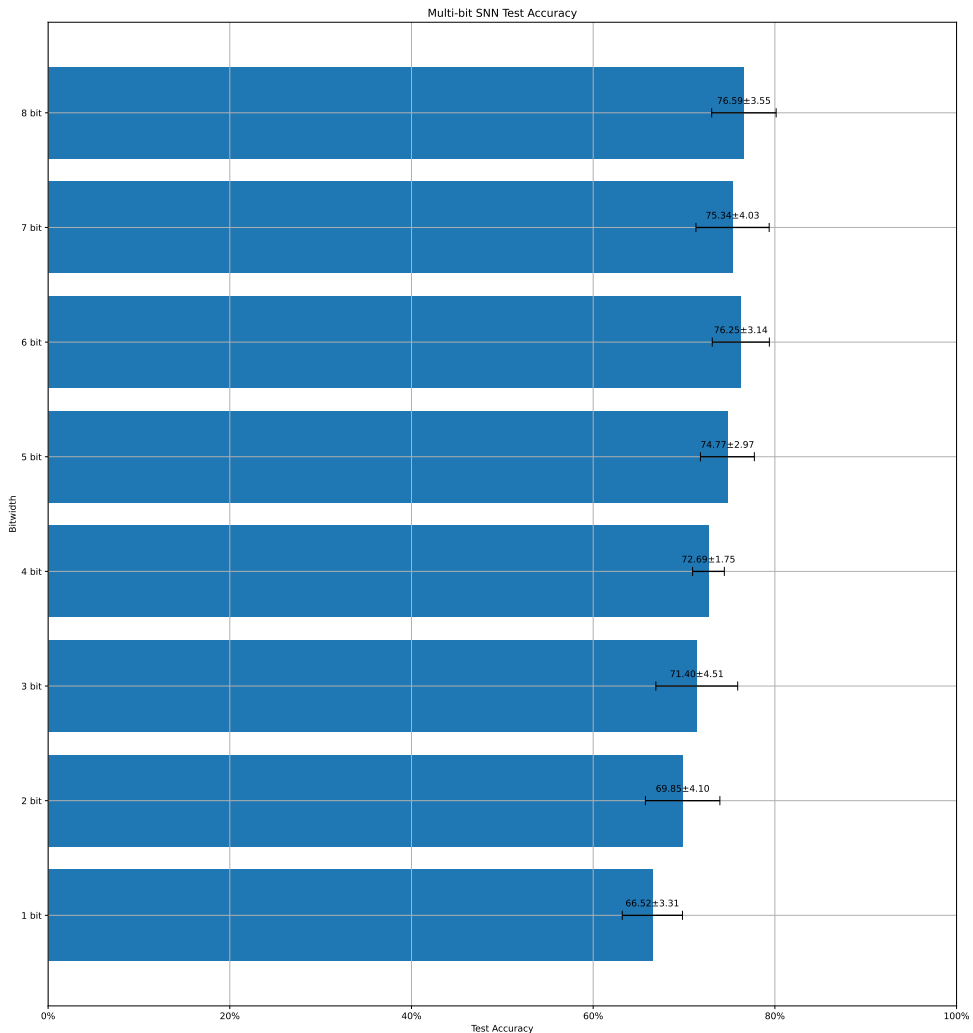


Figure A.12: Final Test Accuracy

A.1.5 CIFAR-10

Launch command:

```
python -m test --N 4 --R 5 --T 10 --acc 0.80 --model
CIFAR10Net --data-path /scratch/zyi/codeSpace/data --
dataset CIFAR10 --batch-size 128 --opt adam --lr 1e-5 --lr
-scheduler none --epochs 50 --lr-warmup-epochs 0 --output-
dir /scratch/zyi/codeSpace/MultibitSpikes
```

A. ACCURACY OF THE MULTI-BIT SPIKE TRAIN MODEL

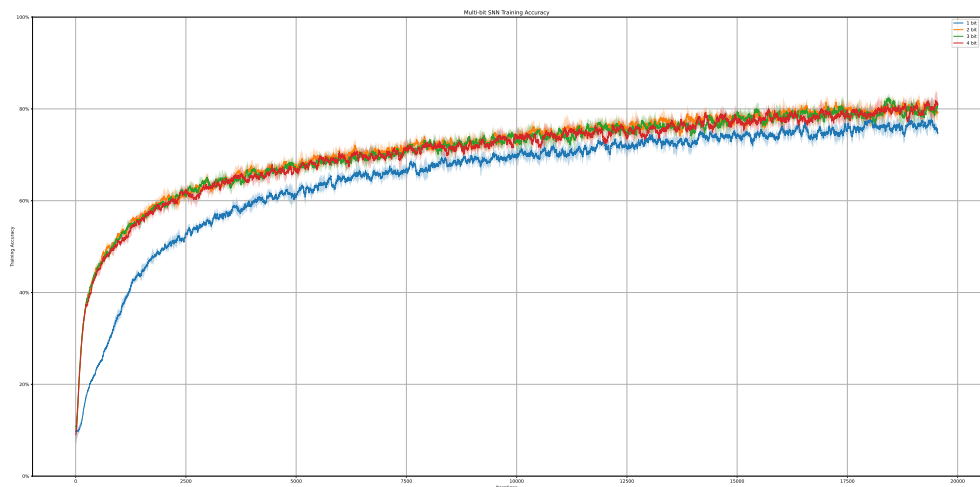


Figure A.13: Training Accuracy (smoothed with a window size of 100)

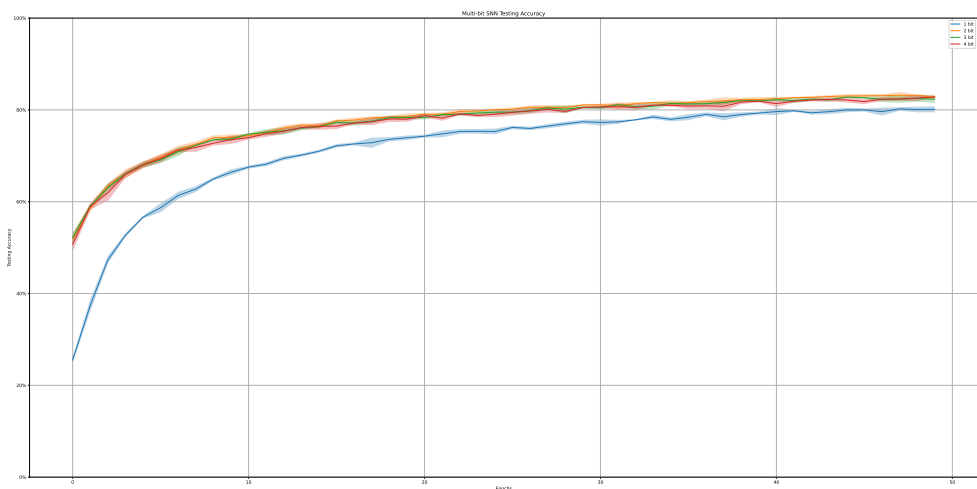


Figure A.14: Test Accuracy

A.2. Iterations to Reach the Target Accuracy of 80%

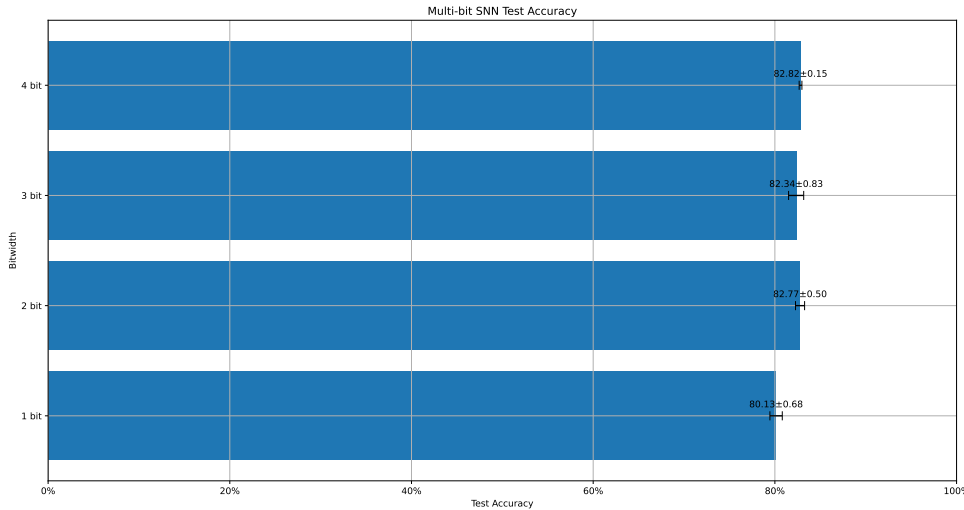


Figure A.15: Final Test Accuracy

A.2 Iterations to Reach the Target Accuracy of 80%

A.2.1 Fashion MNIST

Launch command: Same as in Appendix A.1.1

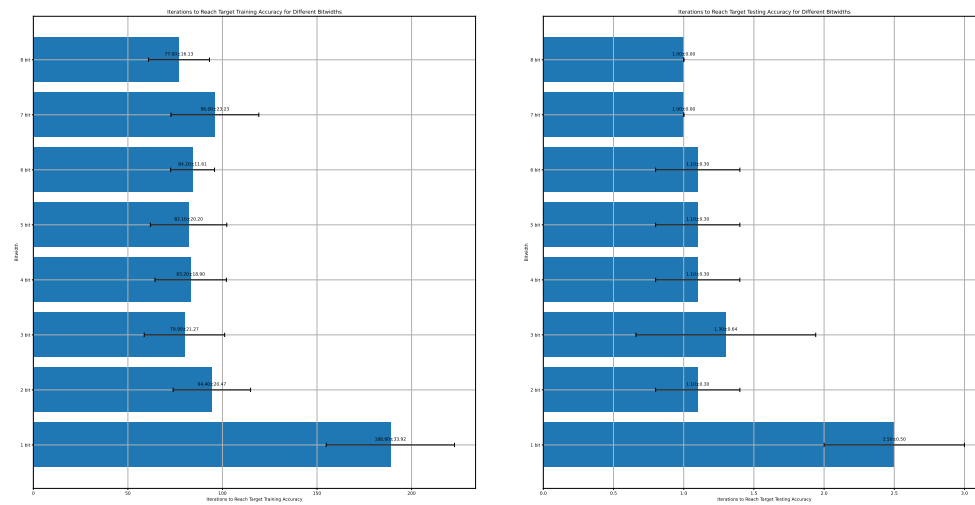


Figure A.16: Iterations to Reach the Target Accuracy of 80%

A.2.2 MNIST

Launch command: Same as in Appendix A.1.2

A. ACCURACY OF THE MULTI-BIT SPIKE TRAIN MODEL

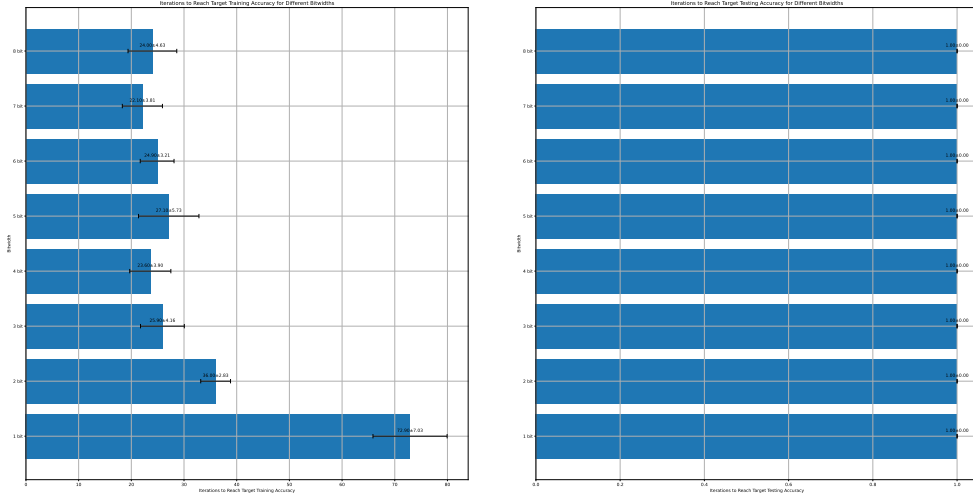


Figure A.17: Iterations to Reach the Target Accuracy of 80%

A.2.3 MNIST

Launch command: Same as in Appendix A.1.3

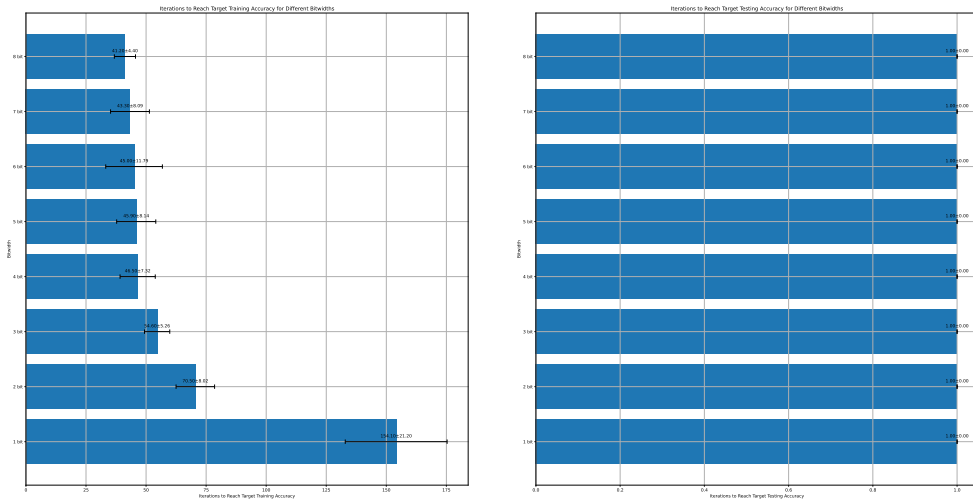
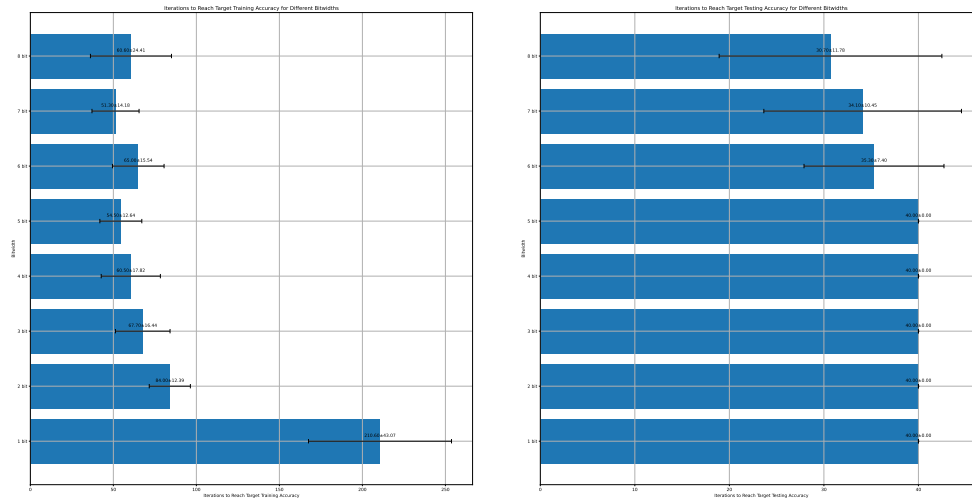


Figure A.18: Iterations to Reach the Target Accuracy of 80%

A.2.4 DVS Gesture

Launch command: Same as in Appendix A.1.4

A.2. Iterations to Reach the Target Accuracy of 80%



(a) Iterations to Reach the Training Accuracy

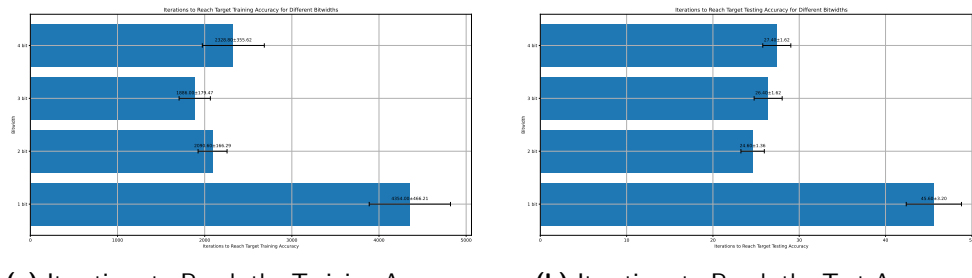
(b) Iterations to Reach the Test Accuracy

Figure A.19: Iterations to Reach the Target Accuracy of 80%

Notice that we encountered overfitting in the DVS Gesture dataset, which is why the number of iterations to reach the target test accuracy is capped at 40 epochs (the maximum number of epochs in the training process), thus not representative.

A.2.5 CIFAR-10

Launch command: Same as in Appendix A.1.5



(a) Iterations to Reach the Training Accuracy

(b) Iterations to Reach the Test Accuracy

Figure A.20: Iterations to Reach the Target Accuracy of 80%

Appendix B

Firing Rate in Different Positions of the Multi-Bit Spike Train Model

For the ease of debugging, the first measuring position is always just the input data. If the data is captured by a dynamic vision sensor or it is encoded with a Poisson spike generator, one should see a firing rate much below 100%. In the case of original data (e.g. CIFAR-10), the firing rate should be close to 100%.

From the second measuring position to the last position, the firing rate is measured after the LIF neuron layers. Not all LIF neuron layers are measured. But the last LIF neuron layer is always measured.

B.1 Fashion MNIST

Launch command:

```
python -m test --N 2 --R 10 --T 10 10 --acc 0.80 --model
    FashionMNISTNet --data-path /scratch/zhiyi/codeSpace/data --
        dataset FashionMNIST --batch-size 128 --opt adam --lr 2e-3
        --lr-scheduler none --epochs 50 --lr-warmup-epochs 0 --
        output-dir /scratch/zhiyi/codeSpace/MultibitSpikes/firerate
        --mixup-alpha 0.0 --cutmix-alpha 0.0 --label-smoothing 0.0
        --disable-amp
```

B. FIRING RATE IN DIFFERENT POSITIONS OF THE MULTI-BIT SPIKE TRAIN MODEL

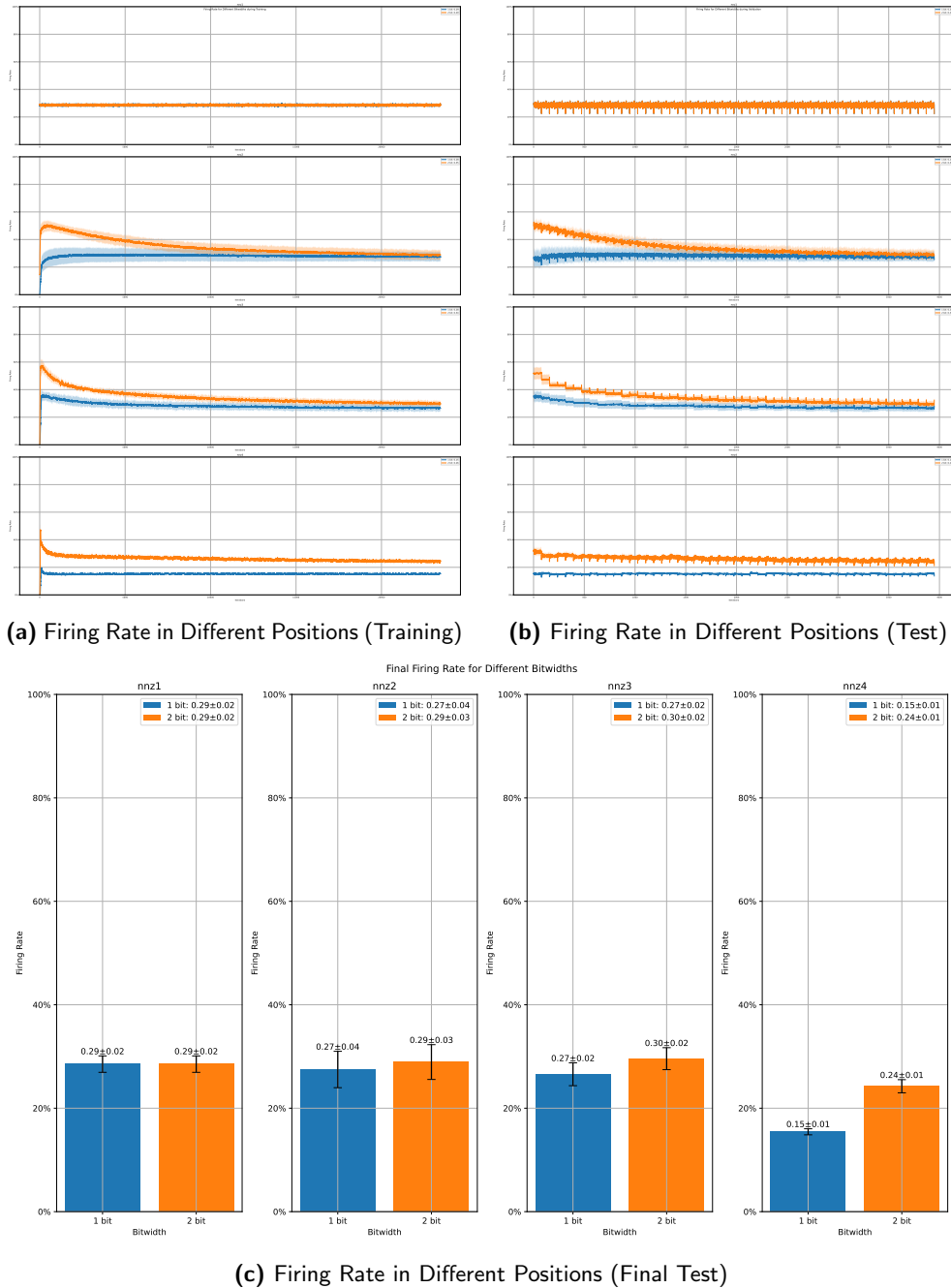


Figure B.1: Firing Rate in Different Positions of the Fashion MNIST Model

B.2 MNIST

Launch command:

```
python -m test --N 2 --R 10 --T 10 10 --acc 0.80 --model  
    MNISTNet --data-path /scratch/zyi/codeSpace/data --dataset  
        MNIST --batch-size 128 --opt adam --lr 2e-3 --lr-  
        scheduler none --epochs 50 --lr-warmup-epochs 0 --output-  
        dir /scratch/zyi/codeSpace/MultibitSpikes/firerate --mixup  
        -alpha 0.0 --cutmix-alpha 0.0 --label-smoothing 0.0 --  
        disable-amp
```

B. FIRING RATE IN DIFFERENT POSITIONS OF THE MULTI-BIT SPIKE TRAIN MODEL

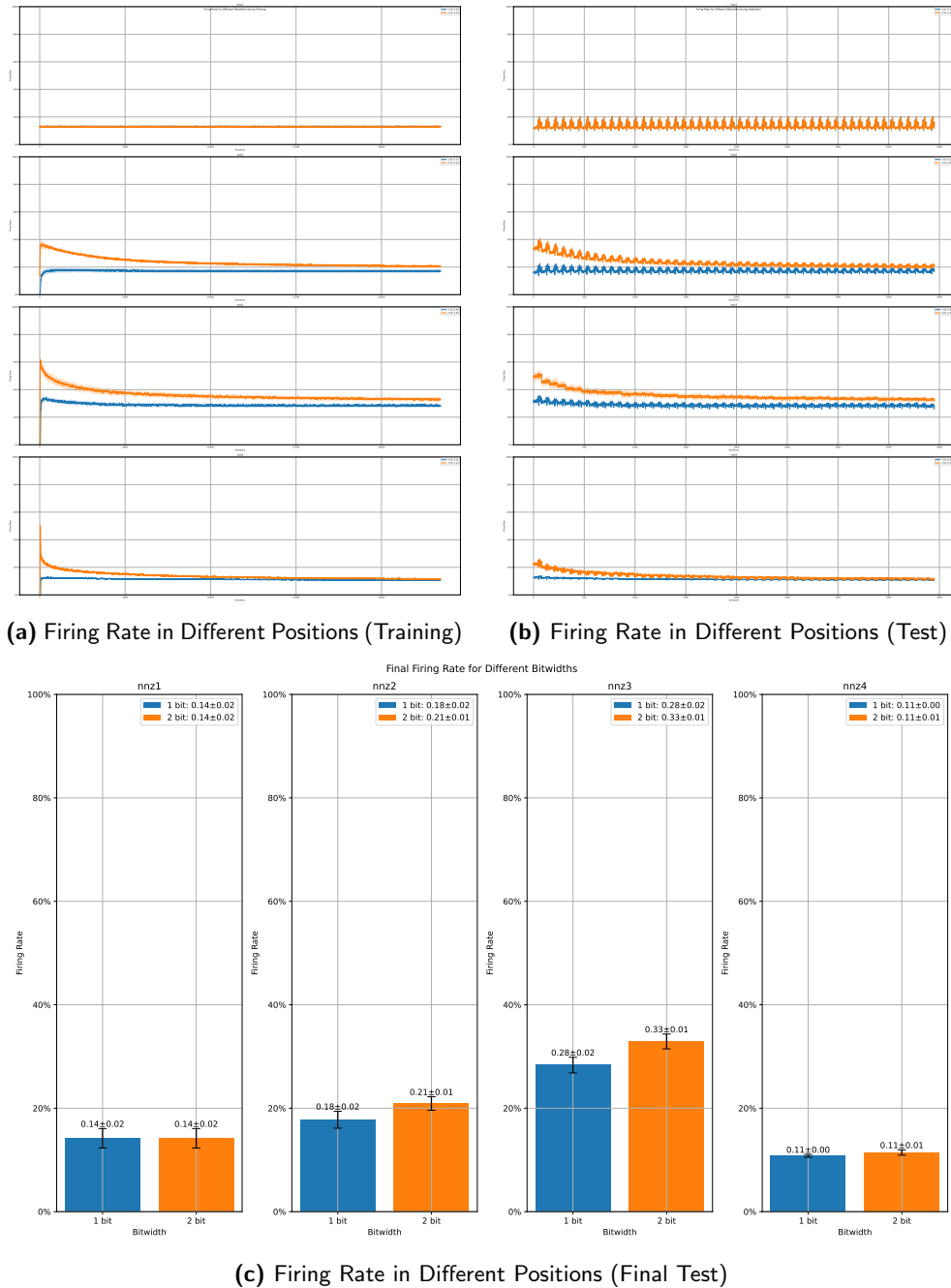


Figure B.2: Firing Rate in Different Positions of the MNIST Model

B.3 NMNIST

Launch command:

```
python -m test --N 2 --R 10 --T 10 10 --acc 0.80 --model  
    NMNISTNet --data-path /scratch/zyi/codeSpace/data --  
    dataset NMNIST --batch-size 128 --opt adam --lr 2e-3 --lr-  
    scheduler none --epochs 50 --lr-warmup-epochs 0 --output-  
    dir /scratch/zyi/codeSpace/MultibitSpikes/firerate --mixup  
    -alpha 0.0 --cutmix-alpha 0.0 --label-smoothing 0.0 --  
    disable-amp
```

B. FIRING RATE IN DIFFERENT POSITIONS OF THE MULTI-BIT SPIKE TRAIN MODEL

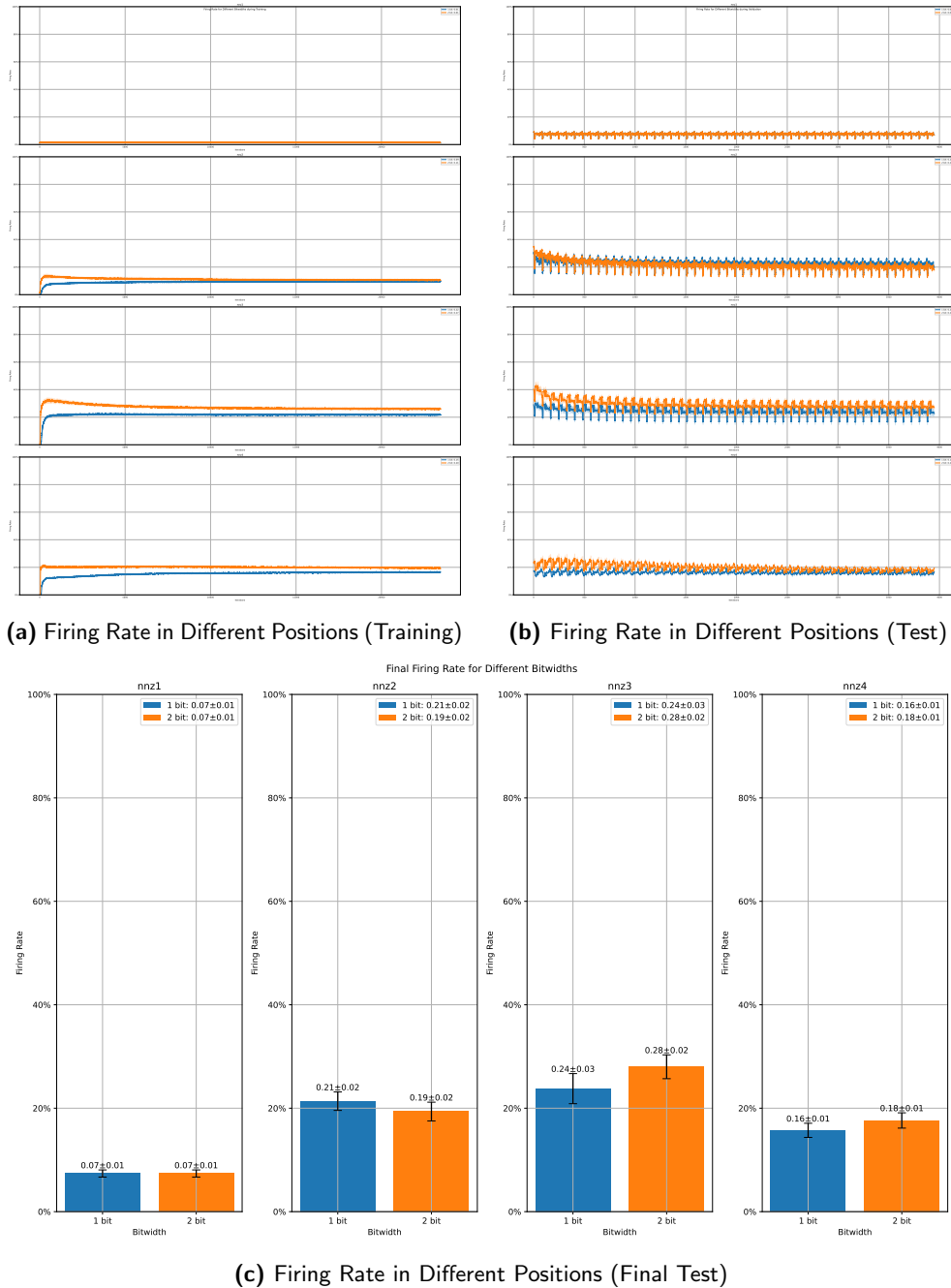


Figure B.3: Firing Rate in Different Positions of the NMNIST Model

B.4 DVS Gesture

Launch command:

```
python -m test --N 2 --R 10 --T 10 10 --acc 0.80 --model  
    DVSGestureNet --data-path /scratch/zyi/codeSpace/data --  
    dataset DVSGesture --batch-size 128 --opt adam --lr 1e-3  
    --lr-scheduler cosa --epochs 200 --lr-warmup-epochs 0 --  
    output-dir /scratch/zyi/codeSpace/MultibitSpikes/firerate
```

The results of experiments on DVS Gesture dataset are the only exception against our conclusion. We suspect that our model is overfitting the training data such that the multi-bit spike train model and the 1-bit spike train model are not generalizing the same way.

B. FIRING RATE IN DIFFERENT POSITIONS OF THE MULTI-BIT SPIKE TRAIN MODEL

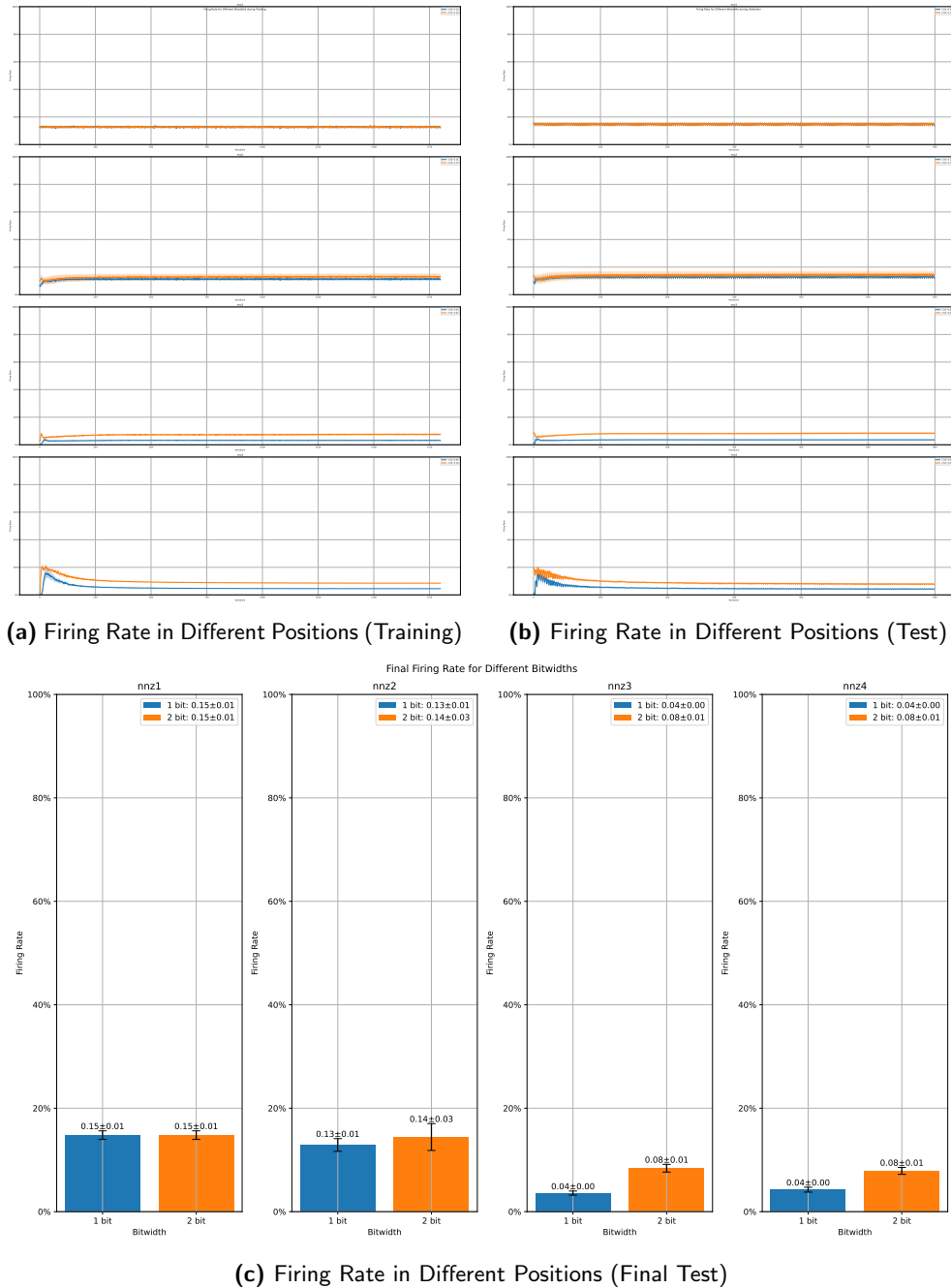


Figure B.4: Firing Rate in Different Positions of the DVS Gesture Model

B.5 CIFAR-10

Launch command:

```
python -m test --N 2 --R 5 --T 10 10 --acc 0.80 --model  
    CIFAR10Net --data-path /scratch/zyi/codeSpace/data --  
    dataset CIFAR10 --batch-size 128 --opt adam --lr 1e-5 --lr  
    -scheduler none --epochs 1000 --lr-warmup-epochs 0 --  
    output-dir /scratch/zyi/codeSpace/MultibitSpikes/firerate
```

Here we use learning rate schedulers to accelerate the convergence of the models. Although the models can reach a high accuracy faster, the multi-bit spike train model suffers from the high learning rate from time to time.

B. FIRING RATE IN DIFFERENT POSITIONS OF THE MULTI-BIT SPIKE TRAIN MODEL

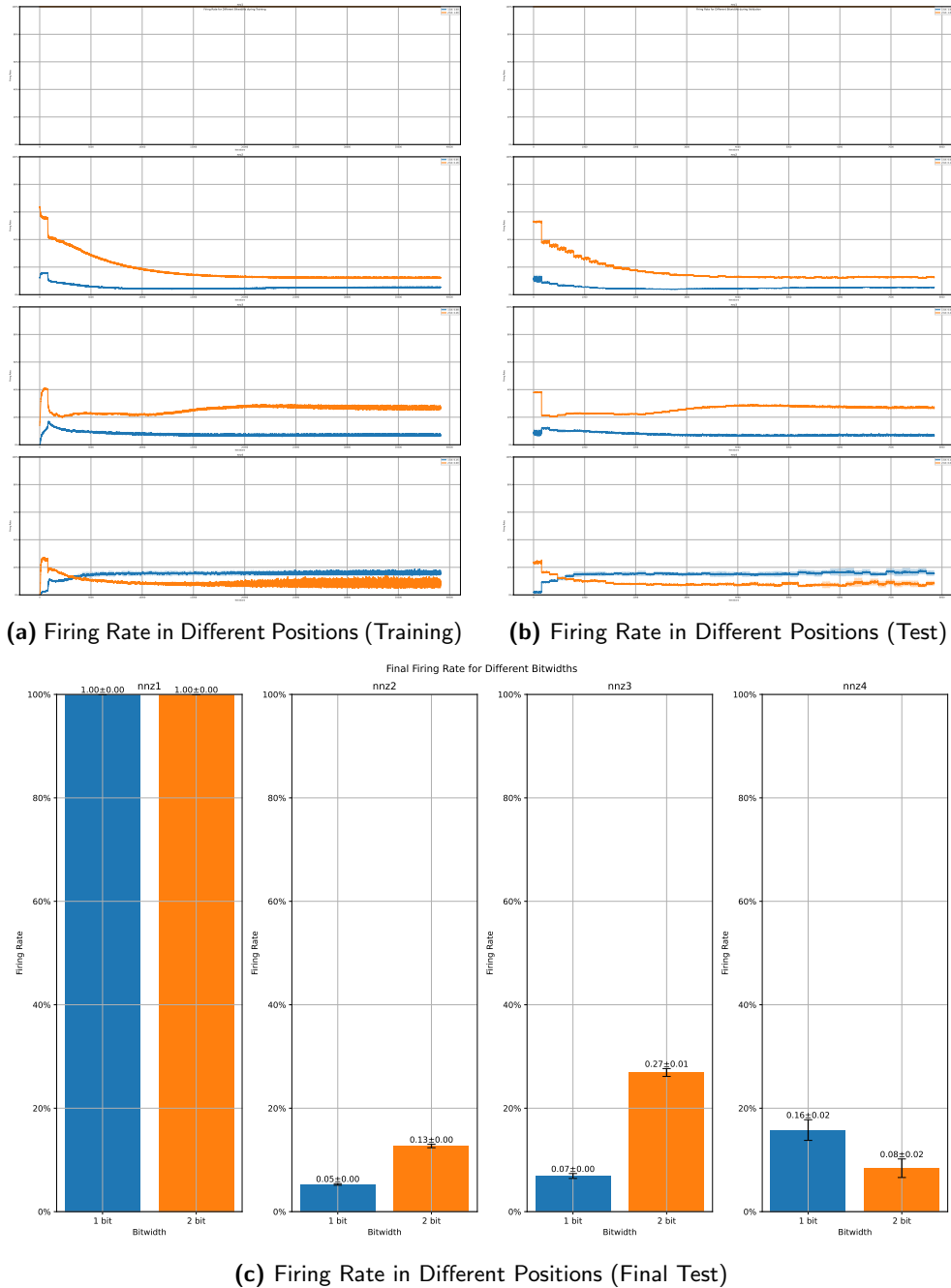


Figure B.5: Firing Rate in Different Positions of the CIFAR-10 Model

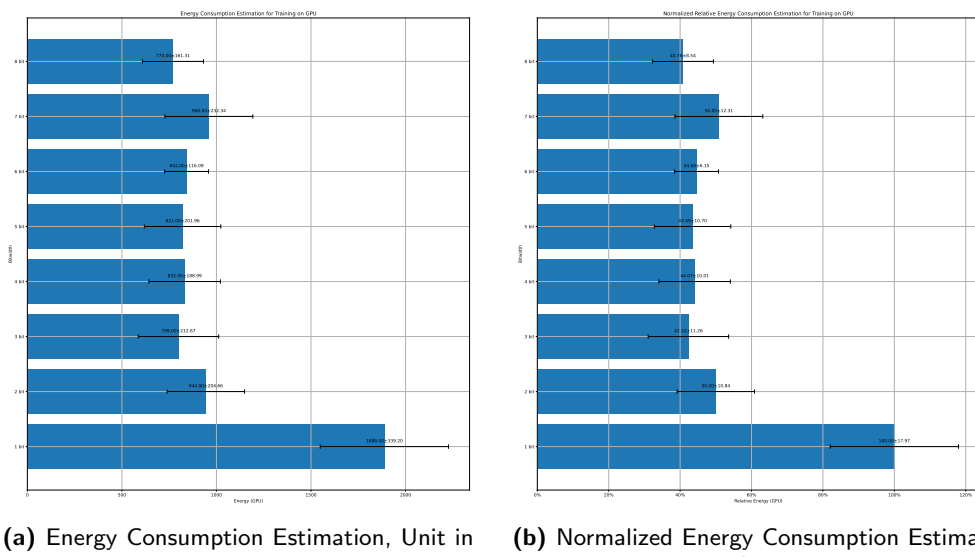
Appendix C

Energy Consumption Estimation

C.1 Training Energy Consumption Estimation on GPUs

C.1.1 Fashion MNIST

Launch command: Same as in Appendix A.1.1



(a) Energy Consumption Estimation, Unit in Constant c

(b) Normalized Energy Consumption Estimation Relative to 1-bit Spike Train Model

Figure C.1: Training Energy Consumption Estimation on GPUs for Fashion MNIST Dataset

C.1.2 MNIST

Launch command: Same as in Appendix A.1.2

C. ENERGY CONSUMPTION ESTIMATION

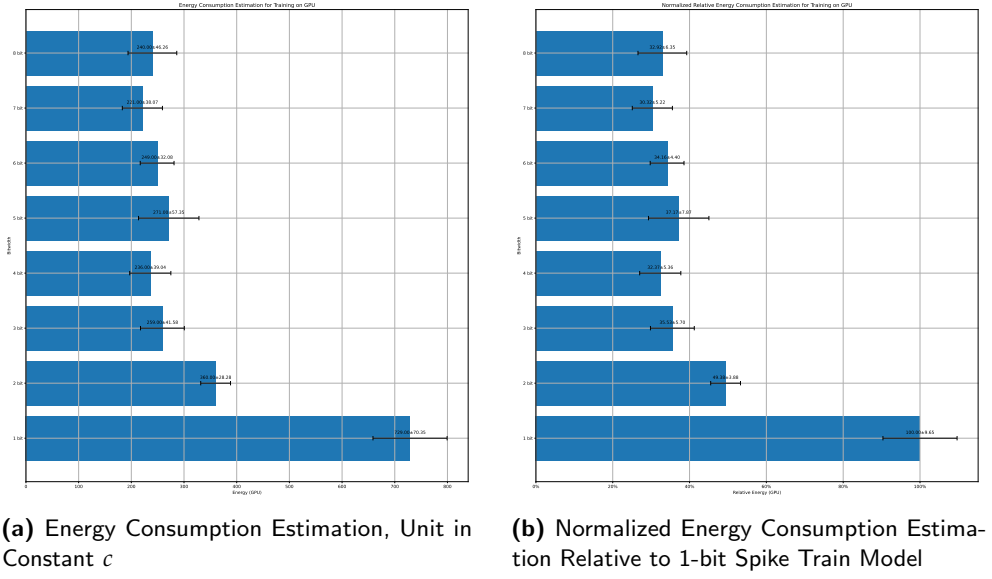


Figure C.2: Training Energy Consumption Estimation on GPUs for MNIST Dataset

C.1.3 NMNIST

Launch command: Same as in Appendix A.1.3

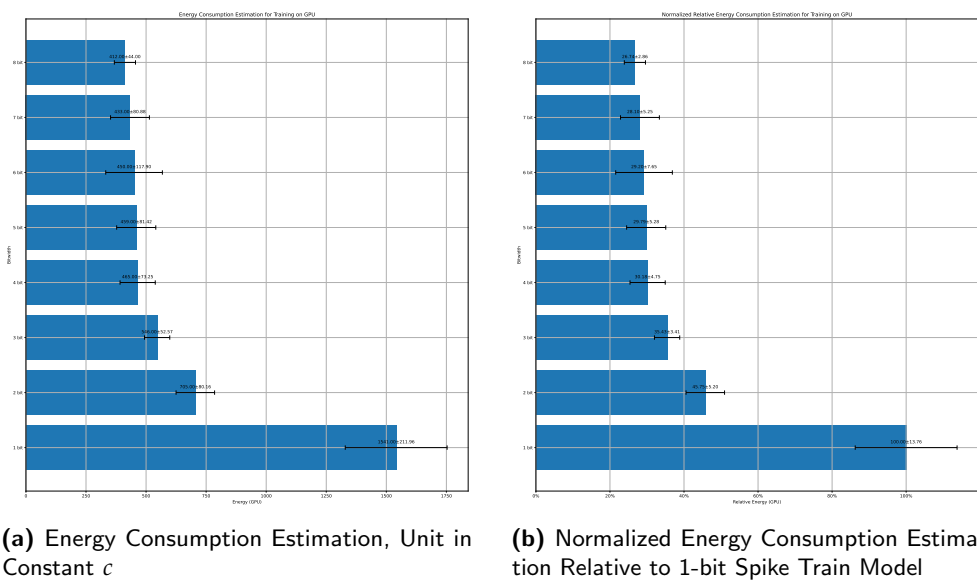


Figure C.3: Training Energy Consumption Estimation on GPUs for NMNIST Dataset

C.2. Inference Energy Consumption Estimation on Neuromorphic Hardware

C.1.4 DVS Gesture

Launch command: Same as in Appendix A.1.4

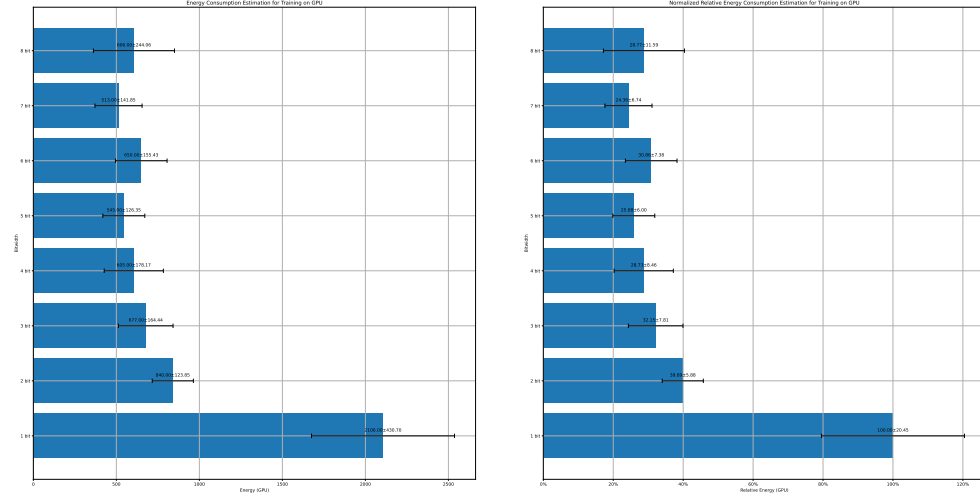


Figure C.4: Training Energy Consumption Estimation on GPUs for DVS Gesture Dataset

C.1.5 CIFAR-10

Launch command: Same as in Appendix A.1.5

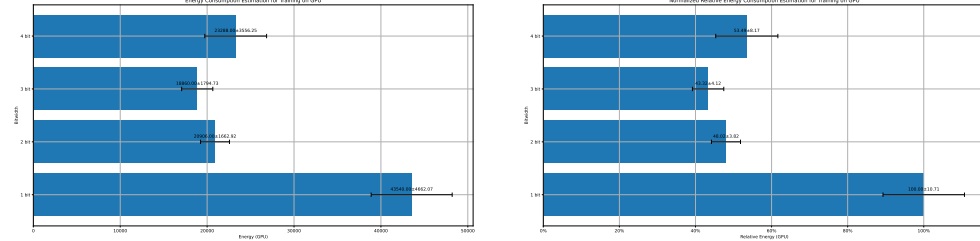


Figure C.5: Training Energy Consumption Estimation on GPUs for CIFAR-10 Dataset

C.2 Inference Energy Consumption Estimation on Neuromorphic Hardware

We assume the models are running on neuromorphic hardware like Intel Loihi 2 that support graded spikes.

C. ENERGY CONSUMPTION ESTIMATION

C.2.1 Fashion MNIST

Launch command: Same as in Appendix A.1.1

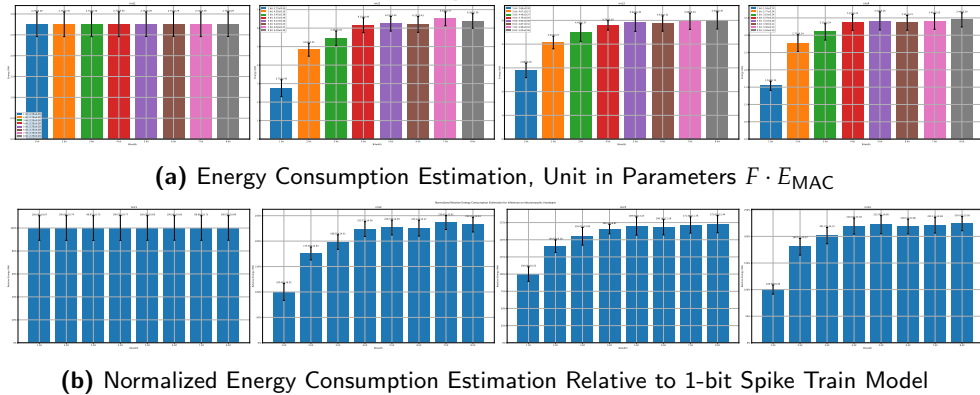


Figure C.6: Inference Energy Consumption Estimation on Intel Loihi 2

C.2.2 MNIST

Launch command: Same as in Appendix A.1.2

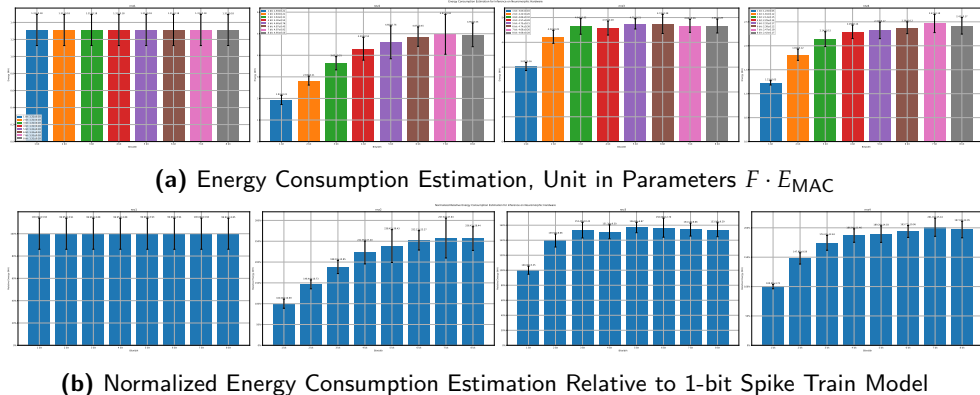


Figure C.7: Inference Energy Consumption Estimation on Intel Loihi 2

6.2.3. MANAGEMENT

Launch command: Same as in Appendix A 1.3

C.2. Inference Energy Consumption Estimation on Neuromorphic Hardware

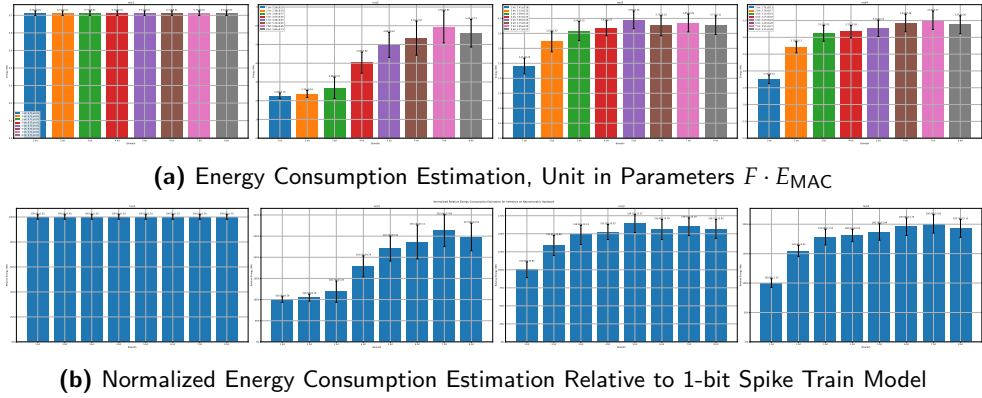


Figure C.8: Inference Energy Consumption Estimation on Intel Loihi 2

C.2.4 DVS Gesture

Launch command: Same as in Appendix A.1.4

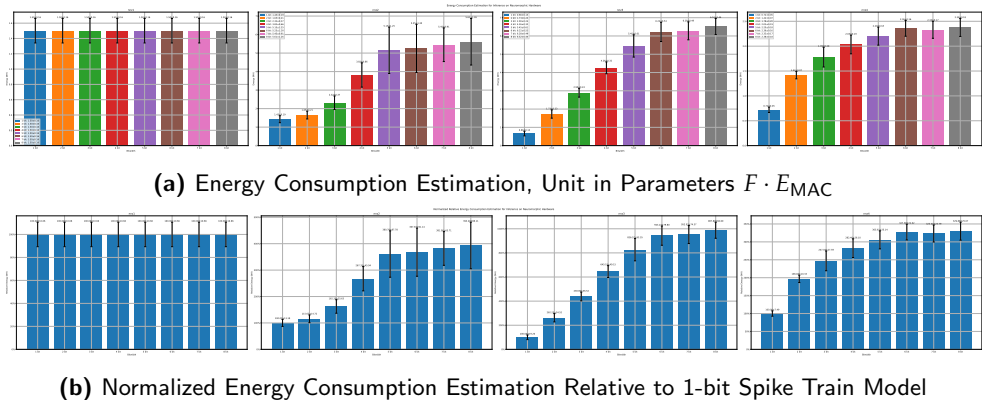


Figure C.9: Inference Energy Consumption Estimation on Intel Loihi 2

C.2.5 CIFAR-10

Launch command: Same as in Appendix A.1.5

C. ENERGY CONSUMPTION ESTIMATION

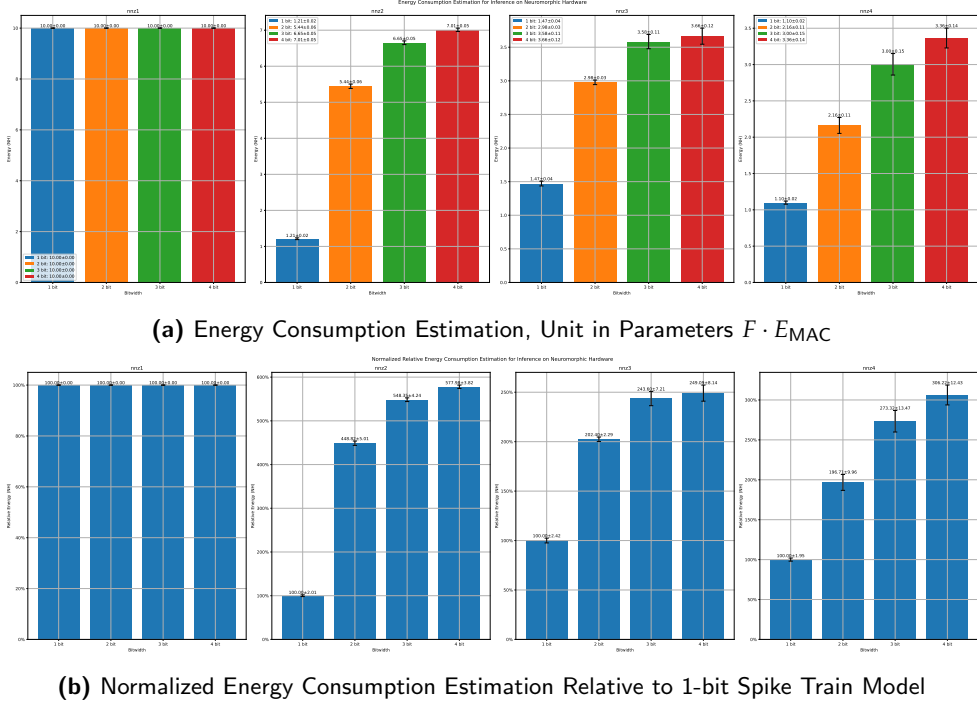


Figure C.10: Inference Energy Consumption Estimation on Intel Loihi 2

C.3 Trading Accuracy for Energy Consumption

C.3.1 Fashion MNIST

Launch command:

```
python -m test --N 2 --R 10 --T 10 4 --acc 0.80 --model
    FashionMNISTNet --data-path /scratch/zyi/codeSpace/data --
    dataset FashionMNIST --batch-size 128 --opt adam --lr 2e-3
    --lr-scheduler none --epochs 5 --lr-warmup-epochs 0 --
    output-dir /scratch/zyi/codeSpace/MultibitSpikes/timesteps
    --mixup-alpha 0.0 --cutmix-alpha 0.0 --label-smoothing
    0.0 --disable-amp
```

C.3. Trading Accuracy for Energy Consumption

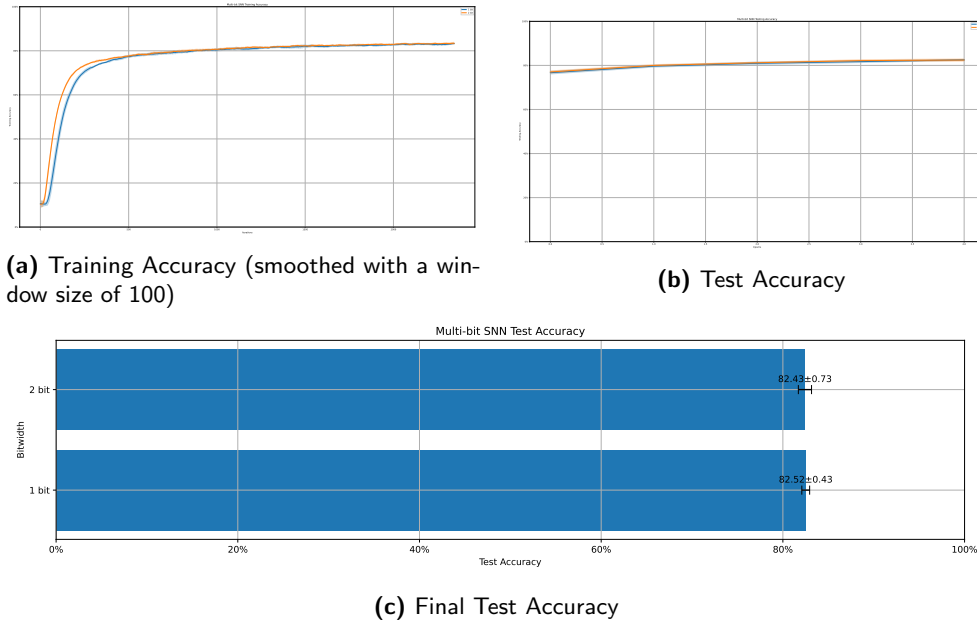


Figure C.11: Accuracy of 1-bit Spike Train Model with 10 Timesteps and 2-bit Spike Train Model with 4 Timesteps

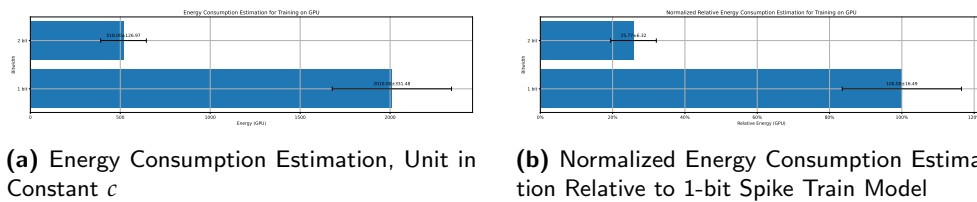


Figure C.12: Training Energy Consumption Estimation on GPUs for Fashion MNIST Dataset

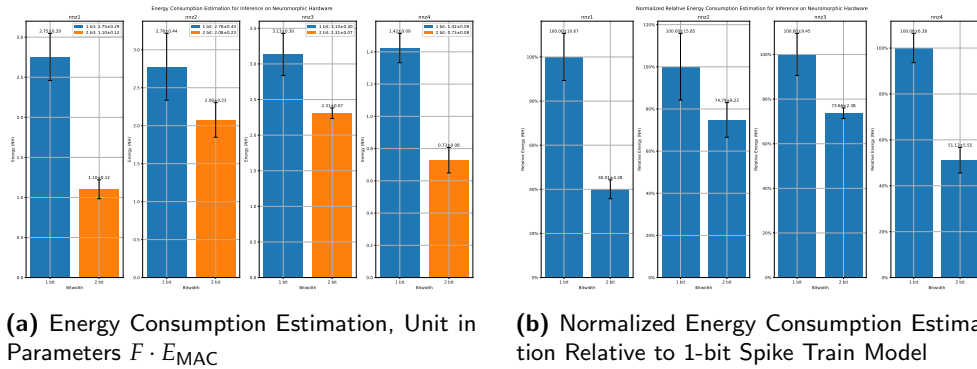


Figure C.13: Inference Energy Consumption Estimation on Intel Loihi 2

C. ENERGY CONSUMPTION ESTIMATION

C.3.2 CIFAR-10

Launch command:

```
python -m test --N 2 --R 5 --T 10 4 --acc 0.80 --model
    CIFAR10Net --data-path /scratch/zyi/codeSpace/data --
    dataset CIFAR10 --batch-size 128 --opt adam --lr 1e-5 --lr-
    scheduler none --epochs 50 --lr-warmup-epochs 0 --output-
    dir /scratch/zyi/codeSpace/MultibitSpikes/timesteps
```

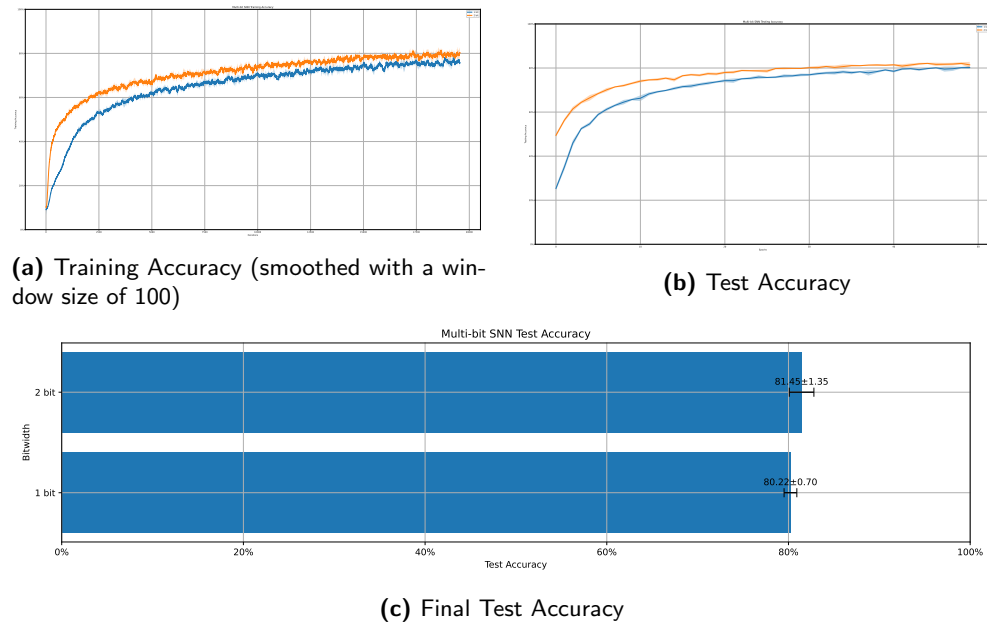


Figure C.14: Accuracy of 1-bit Spike Train Model with 10 Timesteps and 2-bit Spike Train Model with 4 Timesteps

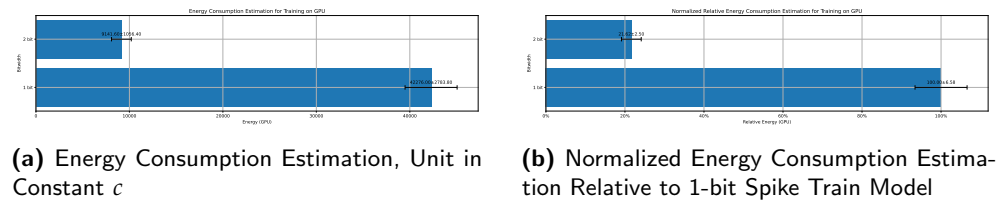


Figure C.15: Training Energy Consumption Estimation on GPUs for CIFAR-10 Dataset

C.3. Trading Accuracy for Energy Consumption

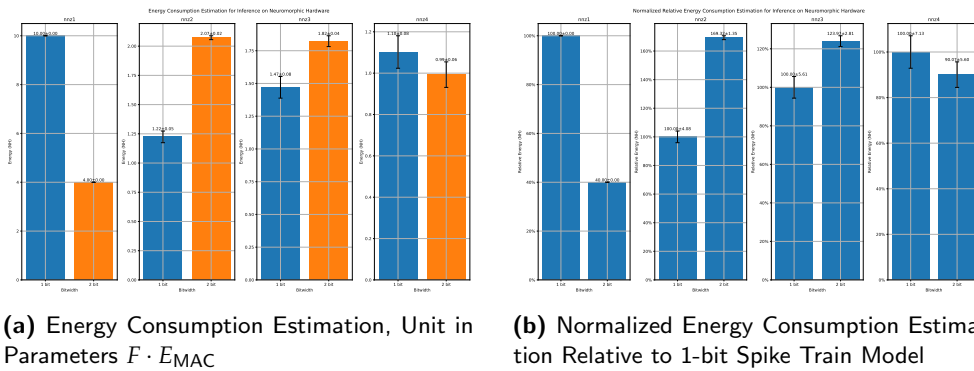


Figure C.16: Inference Energy Consumption Estimation on Intel Loihi 2

Bibliography

- [1] Filipp Akopyan, Jun Sawada, Andrew Cassidy, Rodrigo Alvarez-Icaza, John Arthur, Paul Merolla, Nabil Imam, Yutaka Nakamura, Pallab Datta, Gi-Joon Nam, Brian Taba, Michael Beakes, Bernard Brezzo, Jente B. Kuang, Rajit Manohar, William P. Risk, Bryan Jackson, and Dharmendra S. Modha. Truenorth: Design and tool flow of a 65 mw 1 million neuron programmable neurosynaptic chip. *IEEE Transactions on Computer-Aided Design of Integrated Circuits and Systems*, 34(10):1537–1557, 2015.
- [2] Arnon Amir, Brian Taba, David Berg, Timothy Melano, Jeffrey McKinstry, Carmelo Di Nolfo, Tapan Nayak, Alexander Andreopoulos, Guillaume Garreau, Marcela Mendoza, Jeff Kusnitz, Michael Debole, Steve Esser, Tobi Delbruck, Myron Flickner, and Dharmendra Modha. A low power, fully event-based gesture recognition system. In *2017 IEEE Conference on Computer Vision and Pattern Recognition (CVPR)*, pages 7388–7397, 2017.
- [3] Vijay Balasubramanian. Brain power. *Proceedings of the National Academy of Sciences*, 118(32):e2107022118, 2021.
- [4] Felix Christian Bauer, Gregor Lenz, Saeid Haghshoar, and Sadique Sheik. Exodus: Stable and efficient training of spiking neural networks. *arXiv preprint arXiv:2205.10242*, 2022.
- [5] Steven M. Chase and Eric D. Young. First-spike latency information in single neurons increases when referenced to population onset. *Proceedings of the National Academy of Sciences*, 104(12):5175–5180, 2007.
- [6] Mike Davies, Narayan Srinivasa, Tsung-Han Lin, Gautham Chinya, Yongqiang Cao, Sri Harsha Choday, Georgios Dimou, Prasad Joshi, Nabil Imam, Shweta Jain, Yuyun Liao, Chit-Kwan Lin, Andrew Lines, Ruokun Liu, Deepak Muthaiikutty, Steven McCoy, Arnab Paul, Jonathan

BIBLIOGRAPHY

- Tse, Guruguhanathan Venkataramanan, Yi-Hsin Weng, Andreas Wild, Yoonseok Yang, and Hong Wang. Loihi: A neuromorphic manycore processor with on-chip learning. *IEEE Micro*, 38(1):82–99, 2018.
- [7] Alex de Vries. The growing energy footprint of artificial intelligence. *Joule*, 7(10):2191–2194, 2023.
 - [8] Li Deng. The mnist database of handwritten digit images for machine learning research. *IEEE Signal Processing Magazine*, 29(6):141–142, 2012.
 - [9] Jason K. Eshraghian, Max Ward, Emre O. Neftci, Xinxin Wang, Gregor Lenz, Girish Dwivedi, Mohammed Bennamoun, Doo Seok Jeong, and Wei D. Lu. Training spiking neural networks using lessons from deep learning. *Proceedings of the IEEE*, 111(9):1016–1054, 2023.
 - [10] Wei Fang, Yanqi Chen, Jianhao Ding, Zhaofei Yu, Timothée Masquelier, Ding Chen, Liwei Huang, Huihui Zhou, Guoqi Li, and Yonghong Tian. Spikingjelly: An open-source machine learning infrastructure platform for spike-based intelligence. *Science Advances*, 9(40):eadi1480, 2023.
 - [11] A. L. Hodgkin and A. F. Huxley. A quantitative description of membrane current and its application to conduction and excitation in nerve. *The Journal of Physiology*, 117(4):500–544, 1952.
 - [12] D. H. Hubel and T. N. Wiesel. Receptive fields, binocular interaction and functional architecture in the cat’s visual cortex. *The Journal of Physiology*, 160(1):106–154, 1962.
 - [13] Alex Krizhevsky. Learning multiple layers of features from tiny images. Technical report, 2009.
 - [14] Louis Lapicque. Recherches quantitatives sur l’excitation électrique des nerfs traitée comme une polarization. *J. of Physiol. and Pathology*, 9:620–635, 1907.
 - [15] Gregor Lenz, Kenneth Chaney, Sumit Bam Shrestha, Omar Oubari, Serge Picaud, and Guido Zarrella. Tonic: event-based datasets and transformations., July 2021.
 - [16] Sébastien Marcel and Yann Rodriguez. Torchvision the machine-vision package of torch. In *Proceedings of the 18th ACM International Conference on Multimedia*, MM ’10, page 1485–1488, New York, NY, USA, 2010. Association for Computing Machinery.
 - [17] Warren S McCulloch and Walter Pitts. A logical calculus of the ideas immanent in nervous activity. *The bulletin of mathematical biophysics*, 5(4):115–133, 1943.

Bibliography

- [18] Emre O. Neftci, Hesham Mostafa, and Friedemann Zenke. Surrogate gradient learning in spiking neural networks: Bringing the power of gradient-based optimization to spiking neural networks. *IEEE Signal Processing Magazine*, 36(6):51–63, 2019.
- [19] Kyoungsu Oh and Keechul Jung. Gpu implementation of neural networks. *Pattern Recognition*, 37:1311–1314, 06 2004.
- [20] Garrick Orchard, Ajinkya Jayawant, Gregory K. Cohen, and Nitish Thakor. Converting static image datasets to spiking neuromorphic datasets using saccades. *Frontiers in Neuroscience*, 9, 2015.
- [21] Adam Paszke, Sam Gross, Francisco Massa, Adam Lerer, James Bradbury, Gregory Chanan, Trevor Killeen, Zeming Lin, Natalia Gimelshein, Luca Antiga, Alban Desmaison, Andreas Kopf, Edward Yang, Zachary DeVito, Martin Raison, Alykhan Tejani, Sasank Chilamkurthy, Benoit Steiner, Lu Fang, Junjie Bai, and Soumith Chintala. Pytorch: An imperative style, high-performance deep learning library. In *Advances in Neural Information Processing Systems 32*, pages 8024–8035. Curran Associates, Inc., 2019.
- [22] Rachmad Vidya Wicaksana Putra and Muhammad Shafique. Q-spinn: A framework for quantizing spiking neural networks. In *2021 International Joint Conference on Neural Networks (IJCNN)*, pages 1–8, 2021.
- [23] Abhronil Sengupta, Yuting Ye, Robert Wang, Chiao Liu, and Kaushik Roy. Going deeper in spiking neural networks: Vgg and residual architectures. *Frontiers in Neuroscience*, 13, 2019.
- [24] Sumit Bam Shrestha and Garrick Orchard. SLAYER: Spike layer error re-assignment in time. In S. Bengio, H. Wallach, H. Larochelle, K. Grauman, N. Cesa-Bianchi, and R. Garnett, editors, *Advances in Neural Information Processing Systems 31*, pages 1419–1428. Curran Associates, Inc., 2018.
- [25] Wenjie Wei, Yu Liang, Ammar Belatreche, Yichen Xiao, Honglin Cao, Zhenbang Ren, Guoqing Wang, Malu Zhang, and Yang Yang. Q-snns: Quantized spiking neural networks. In *Proceedings of the 32nd ACM International Conference on Multimedia*, MM ’24, page 8441–8450, New York, NY, USA, 2024. Association for Computing Machinery.
- [26] Han Xiao, Kashif Rasul, and Roland Vollgraf. Fashion-mnist: a novel image dataset for benchmarking machine learning algorithms, 2017.
- [27] Rui-Jie Zhu, Qihang Zhao, Guoqi Li, and Jason K. Eshraghian. Spikegpt: Generative pre-trained language model with spiking neural networks, 2024.

Declaration of originality

The signed declaration of originality is a component of every semester paper, Bachelor's thesis, Master's thesis and any other degree paper undertaken during the course of studies, including the respective electronic versions.

Lecturers may also require a declaration of originality for other written papers compiled for their courses.

I hereby confirm that I am the sole author of the written work here enclosed and that I have compiled it in my own words. Parts excepted are corrections of form and content by the supervisor.

Title of work (in block letters):

Authored by (in block letters):

For papers written by groups the names of all authors are required.

Name(s):

First name(s):

With my signature I confirm that

- I have committed none of the forms of plagiarism described in the '[Citation etiquette](#)' information sheet.
- I have documented all methods, data and processes truthfully.
- I have not manipulated any data.
- I have mentioned all persons who were significant facilitators of the work.

I am aware that the work may be screened electronically for plagiarism.

Place, date

Signature(s)

For papers written by groups the names of all authors are required. Their signatures collectively guarantee the entire content of the written paper.